Imaginary part of the optical potential for preequilibrium processes

K. Sato
Division of Physics, Tohoku College of Pharmacy, Sendai 981, Japan

S. Yoshida
Ishinomaki Senshu University, Ishinomaki 986, Japan
(Received 19 July 1993)

The imaginary part of optical potentials for fixed exciton number to be used for preequilibrium reactions is microscopically calculated. The semiclassical approximation and a simple delta function type interaction are adopted. Only the lowest order processes are taken into account, and the incident particle is restricted to nucleons. Five types of processes contribute to the imaginary potential; the first is the creation of a particle-hole pair by the incident nucleon. This process is considered in usual optical potentials, but in this work the intermediate states are restricted to Q space. The imaginary parts corresponding to the other four processes are obtained in analytic forms, to which the effects of particle-hole states in the target nucleus are taken into account. The resultant imaginary parts are, with good accuracy, independent of the excitation energy and related to the exciton number in a very simple way. The transmission coefficients are calculated using obtained imaginary parts and compared with the ones based on conventional imaginary potentials. The effect of inelastic scattering before absorption is studied in a perturbation expansion and the second-order terms are found to be comparable with the zeroth-order terms.

PACS number(s): 24.10.Ht, 24.60.Dr, 24.60.Gv

I. INTRODUCTION

Optical potentials have been devised to generate energy-averaged elastic scattering amplitudes and applied to numerous analyses of experimental data. Absorption by the imaginary potential is considered to be the formation of a compound nucleus, and the transmission coefficient is calculated to be used for the Hauser-Feshbach statistical theory of nuclear reactions.

With the development of the coupled channel approximation of direct reactions, the optical potential has also been modified to accommodate the situation where certain important channels are taken into account explicitly, while the effects of the remaining channels are treated statistically [1]. Many works on optical potentials for the coupled channel calculations and other processes have been published.

Preequilibrium reaction theories have been utilized to analyze a great deal of nuclear reaction data, but only after the work of Feshbach *et al.* [2] did the function of the optical potential in this process become clear. The whole Hilbert space is divided into two parts, the P space where at least one nucleon is in a continuum state, and the Q space where all nucleons are bound. Both P and Q spaces are further divided according to the exciton number, which is a sum of the excited particle and hole numbers.

The incident particle proceeds in the P space exciting the target nucleus and if it loses enough energy it falls in the Q space. In the Q space, nucleons collide with other nucleons changing the exciton number, and at some stage one nucleon gets enough energy to be ejected before reaching equilibrium. The reaction which takes place in the P space is called the multistep direct (MSD) reaction, while the reaction in the Q space is the multistep compound (MSC) reaction.

Bonetti *et al.* [3] analyzed experimental data successfully using the MSC theory of Feshbach *et al.* [2]. Recently Chadwick and Young [4] calculated both MSD and MSC reaction cross sections simultaneously and found that the MSC cross section must be reduced to fit the experimental data if the conventional optical potential is used to calculate the transmission coefficient.

On the other hand, Nishioka *et al.* [5] gave a fully quantum mechanical and microscopic foundation for the MSC reaction theory based on the random matrix theory. That theory was previously used in the equilibrium case [6] and it was shown that the fluctuation cross section is expressed in terms of transmission coefficients which are obtained from the optical potentials fitted to the elastic and total cross sections and no further information was necessary. In the preequilibrium process (MSC), this is not the case and further work was necessary in order to analyze the experimental data. This was carried out by Herman, Reffo, and Weidenmüller [7], who obtained a good agreement with the experimental data. They made assumptions to calculate the necessary transmission coefficients from the available optical potentials. To evaluate the MSC reaction cross section based on the quantum mechanical theory [5] more closely and to check the validity of their assumptions, it is desirable to calculate optical potentials microscopically.

In this paper the imaginary part of the optical potential for preequilibrium processes is studied. Microscopic optical potentials have been investigated in various ways, but the semiclassical one is simple and also suitable for

preequilibrium processes because the average potential is obtained. The Thomas-Fermi theory gives optical potentials averaged over the energy as well as the mass number [8]. This is nice since the preequilibrium model describes bulk nuclear properties. As the dependence of optical potentials on the angular momentum is usually known to be weak, it is reasonable to use the momentum representation, which is much easier to handle. We can avoid the need to calculate the transmission coefficients for each partial wave microscopically as was done by Feshbach *et al.* [2].

We use the Thomas-Fermi theory as a basis and employ a simple residual interaction of a delta-function type. We have to calculate various processes which are not encountered in a usual optical potential calculation except for the finite temperature optical potential [9]. We take into account only the lowest-order processes, and restrict the incident particle to nucleons. Our aim is just to explore the new area and study the bulk properties of the imaginary potential. Of course, more refined and detailed studies for a particular nucleus may be necessary but we do not attempt these in this paper.

In the following section, five kinds of processes for target states with a minimum number of excitons, which we call elementary processes, will be investigated. The calculation is not difficult but the integration over the phase space is rather tedious, so details of these calculations are included in appendixes. The obtained results will be compared with previous works. In Sec. III, the imaginary potential in a general case is considered, where the effect of the spectator is taken into account. The exciton number and excitation energy dependence of the imaginary potential will be discussed. In Sec. IV, the transmission coefficients to be used in a preequilibrium process are calculated. The effect of indirect capture will also be estimated. In the last section, the summary and discussion will be presented. In the appendixes, a detailed derivation of the integrals which appeared in the imaginary potential for elementary processes is presented.

II. ELEMENTARY PROCESSES

In the MSC process, the target or residual nucleus is, in general, in an excited state with a certain exciton number, so the imaginary potential is calculated taking into account this fact. As the nucleon-nucleon interaction is assumed to be two-body in nature, the nucleons in the target nucleus may be divided into two groups, the participant, which interacts with the incident nucleon, and the spectator. The process which takes place between the incident nucleon and the participant is called the elementary process here. The spectator does nothing except for sharing the excitation energy. In this section the imaginary potential for the elementary processes is calculated.

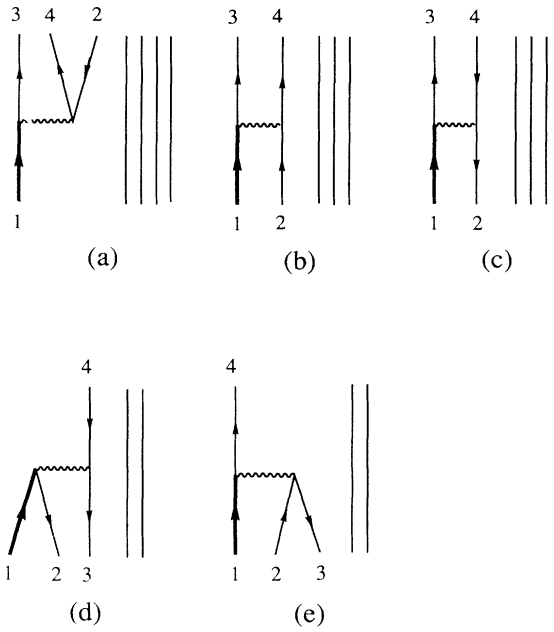

FIG. 1. The five types of processes contributing to the imaginary potentials.

There are five types of elementary processes, and the first is the creation of a particle-hole pair, which appears in usual optical potentials. The calculation is the same as that given by [8] except for the domain of particle states. We follow their procedure to introduce the Thomas-Fermi approximation.

A. Creation of a particle-hole pair

The process is shown in Fig. 1(a). The imaginary part of the mass operator for the polarization effect is given by

$$\langle 1|w^{(a)}|1\rangle = \mathrm{Im}\lim_{\delta\to 0}\frac{1}{2}\sum_{234}\frac{\langle 12|v|34\rangle n_h(2)n_p(3)n_p(4)\langle 43|v|21\rangle}{E_1+E_2-E_3-E_4+i\delta}. \tag{2.1}$$

The numbers 1,2,... represent the variables for the single particle or hole, namely, the coordinate vector $\mathbf{r}_i$, and the spin and isospin variables are represented by a single symbol s_i. The single particle energy is given by E_i, and the occupation probability for a particle by $n_p(i)$ and for a hole by $n_h(i)$. The mass operator Eq. (2.1) is written as

$$\langle 1|w^{(a)}|1\rangle = -\frac{\pi}{2}\sum_{s_2\cdots s_{4'}}\int d\mathbf{r}_2 d\mathbf{r}_3 d\mathbf{r}_4 d\mathbf{r}_{4'} d\mathbf{r}_{3'} d\mathbf{r}_{2'}\frac{dt}{2\pi\hbar}e^{iE_1t/\hbar}\langle 12|v|34\rangle$$
$$\times\langle 2|\hat{\rho}_h e^{iht/\hbar}|2'\rangle\langle 3|\hat{\rho}_p e^{-iht/\hbar}|3'\rangle\langle 4|\hat{\rho}_p e^{-iht/\hbar}|4'\rangle\langle 4'3'|v|2'1\rangle, \tag{2.2}$$

where $\hat{\rho}_p$ is the single particle density operator and $\hat{\rho}_h$ the single hole one, while h is the single particle Hamiltonian. Next, the Thomas-Fermi-like approximation for the single particle density is introduced by

$$\langle \mathbf{r}s|\hat{\rho}_p e^{-iht/\hbar}|\mathbf{r}'s'\rangle = \delta_{ss'}\int \frac{d\mathbf{P}}{(2\pi)^3} e^{-i\mathbf{P}(\mathbf{r}-\mathbf{r}')} \times e^{-iE[\mathbf{P},(\mathbf{r}+\mathbf{r}')/2]t/\hbar} \times n_p\left[E\left(\mathbf{P},\frac{\mathbf{r}+\mathbf{r}'}{2}\right)\right], \tag{2.3}$$

where the single particle energy for the wave number $\mathbf{P}$ at the location $\mathbf{R}$ is given by

$$E(\mathbf{P},\mathbf{R}) = \frac{\hbar^2 P^2}{2m^*(R)} + U(R). \tag{2.4}$$

The single particle energy is a sum of kinetic and potential energy, and the effective mass $m^*(R)$ is introduced to take into account the energy dependence of the mean potential, although our choice of a zero-range interaction has no such energy dependence. We also restrict ourselves to the case of being on the energy shell. The mean field $U(R)$ and the effective mass are adopted independent of our choice of the nucleon-nucleon interaction to simplify the calculation.

The occupation probability of particle and hole are given by

$$n_p(E) = \Theta(E-E_F)\Theta(E_0-E), \tag{2.5a}$$

$$n_h(E) = \Theta(E_F-E), \tag{2.5b}$$

where $\Theta(x)$ is the unit step function, E_F represents the Fermi energy, and E_0 is the upper limit of the particle energy. In the usual optical model $E_0=\infty$ is used. We assume that E_F, E_0 are same for neutrons and protons, and take $E_0 = 0$ except for the cases where it is otherwise stated. For the incident particle $E_F \le E_1$ is assumed, and usually $E_0 \le E_1$ but also the opposite case $E_1 \le E_0$ is considered for completeness.

The nucleon-nucleon interaction is assumed to be zero range and spin independent, and its matrix element is expressed as

$$\langle 12|v|34\rangle = \delta(\mathbf{r}_1-\mathbf{r}_3)\delta(\mathbf{r}_2-\mathbf{r}_4)\delta(\mathbf{r}_1-\mathbf{r}_2)v_{s_1s_2,s_3s_4}(r_1), \tag{2.6}$$

where

$$v_{s_1s_2,s_3s_4}(R) = v_0(R)\langle s_1s_2|1-P_\sigma P_\tau|s_3s_4\rangle. \tag{2.7}$$

In the above equation P_σ and P_τ represent the exchange operator of spins and isospins, respectively. Now, the Wigner transform of the imaginary part of the optical potential is calculated by

$$w^{(a)}_{ss'}(E,\mathbf{P},\mathbf{R}) = \int d\mathbf{x} e^{i\mathbf{P}\cdot\mathbf{x}}\langle \mathbf{R}+\frac{\mathbf{x}}{2},s|w^{(a)}(E)|\mathbf{R}-\frac{\mathbf{x}}{2},s'\rangle \tag{2.8}$$

as

$$w^{(a)}_{s_1s_1}(\mathbf{P}_1,\mathbf{R}_1) = -\frac{\pi}{2}(2\pi)^{-9}\sum_{s_2s_3s_4}\int \frac{dt}{2\pi\hbar} d\mathbf{x}d\mathbf{P}_2d\mathbf{P}_3d\mathbf{P}_4 v_{s_1s_2,s_3s_4}\left(\mathbf{R}_1+\frac{\mathbf{x}}{2}\right) \times v_{s_4s_3,s_2s_1}\left(\mathbf{R}_1-\frac{\mathbf{x}}{2}\right)\exp\{i(\mathbf{P}_1+\mathbf{P}_2-\mathbf{P}_3-\mathbf{P}_4)\cdot\mathbf{x}\}\exp\Big[i\{E(\mathbf{P}_1,\mathbf{R}_1)+E(\mathbf{P}_2,\mathbf{R}_2) -E(\mathbf{P}_3,\mathbf{R}_3)-E(\mathbf{P}_4,\mathbf{R}_4)\}t/\hbar\Big] n_h[E(\mathbf{P}_2,\mathbf{R}_2)]\,n_p[E(\mathbf{P}_3,\mathbf{R}_3)]\,n_p[E(\mathbf{P}_4,\mathbf{R}_4)]. \tag{2.9}$$

Sums over intermediate spin and isospin states are performed assuming $N=Z$,

$$\sum_{s_2s_3s_4} v_{s_1s_2,s_3s_4}\left(\mathbf{R}_1+\frac{\mathbf{x}}{2}\right)v_{s_4s_3,s_2s_1}\left(\mathbf{R}_1-\frac{\mathbf{x}}{2}\right) = v_0\left(\mathbf{R}_1+\frac{\mathbf{x}}{2}\right)v_0\left(\mathbf{R}_1-\frac{\mathbf{x}}{2}\right) \times\sum_{s_2}\langle s_1s_2|(1-P_\sigma P_\tau)^2|s_1s_2\rangle = 6v_0\left(\mathbf{R}_1+\frac{\mathbf{x}}{2}\right)v_0\left(\mathbf{R}_1-\frac{\mathbf{x}}{2}\right)\approx 6[v_0(\mathbf{R}_1)]^2, \tag{2.10}$$

where the last expression is supposed to be a good approximation. If this is put in Eq. (2.9) we obtain

$$w^{(a)}(\mathbf{P}_1,\mathbf{R}_1) = -\frac{\pi}{2}(2\pi)^{-6}6[v_0(R_1)]^2\int d\mathbf{P}_2d\mathbf{P}_3d\mathbf{P}_4\delta(\mathbf{P}_1+\mathbf{P}_2-\mathbf{P}_3-\mathbf{P}_4) \times\delta\Big\{E(\mathbf{P}_1,\mathbf{R}_1)+E(\mathbf{P}_2,\mathbf{R}_2)-E(\mathbf{P}_3,\mathbf{R}_3)-E(\mathbf{P}_4,\mathbf{R}_4)\Big\}n_h(\varepsilon_2)n_p(\varepsilon_3)n_p(\varepsilon_4), \tag{2.11}$$

where the suffix s_1 is dropped as the imaginary potential is independent of s_1.

By defining the Fermi wave number $P_F(R)$ and the upper bound of particle wave number $P_0(R)$ by the following formulas

$$\frac{\hbar^2P_F^2(R)}{2m^*(R)} = E_F - U(R), \qquad \frac{\hbar^2P_0^2(R)}{2m^*(R)} = E_0 - U(R), \tag{2.12}$$

the particle and hole occupation probabilities are given by

$$n_p(P) = \Theta(P-P_F)\Theta(P_0-P), \tag{2.13a}$$

$$n_h(P) = \Theta(P)\Theta(P_F-P). \tag{2.13b}$$

The imaginary part of the optical potential for process (a) is

$$w^{(a)}(P_1,R_1)=-\frac{\pi}{2}(2\pi)^{-6}\frac{2m^*(R_1)}{\hbar^2}6[v_0(R_1)]^2\int d\mathbf{P}_2d\mathbf{P}_3d\mathbf{P}_4\delta(\mathbf{P_1}+\mathbf{P_2}-\mathbf{P_3}-\mathbf{P_4})$$
$$\times\delta(P_1^2+P_2^2-P_3^2-P_4^2)n_h(P_2)n_p(P_3)n_p(P_4). \tag{2.14}$$

This result is the same as that given by the Fermi-gas model in which momentum and energy conservation are taken into account [10].

Calculation of integrals over wave numbers is given in Appendix A. The final results are

$$w^{(a)}(E_1,R_1)=-\frac{\pi}{2}(2\pi)^{-4}\frac{2m^*(R_1)}{\hbar^2}6[v_0(R_1)]^2\frac{1}{P_1}$$
$$\times\Big[\left\{f(P_\beta^2)-f(P_\alpha^2)\right\}\Theta(P_\beta-P_\alpha)$$
$$+\left\{g(P_\delta^2)-g(P_\gamma^2)\right\}\Theta(P_\delta-P_\gamma)\Big], \tag{2.15}$$

where two functions are defined by

$$f(x)=\left\{\frac{1}{3}(P_0^2-\frac{1}{2}P_1^2)-\frac{1}{10}x\right\}x^{\frac{3}{2}}, \tag{2.16a}$$

$$g(x)=\left\{\frac{1}{3}(\frac{1}{2}P_1^2-P_F^2)+\frac{1}{10}x\right\}x^{\frac{3}{2}} \tag{2.16b}$$

and the limits of P_2^2 are given by

$$P_\alpha^2=\max\{P_0^2+P_F^2-P_1^2,0\}, \tag{2.17a}$$

$$P_\beta^2=\max\left[0,\min\{P_F^2,2P_0^2-P_1^2\}\right], \tag{2.17b}$$

$$P_\gamma^2=\max\{2P_F^2-P_1^2,0\}, \tag{2.17c}$$

$$P_\delta^2=\max\left[0,\min\{P_F^2+P_0^2-P_1^2,P_F^2\}\right]. \tag{2.17d}$$

From Eqs. (2.17b) and (2.17d) it follows that $P_\beta^2=0$ and $P_\delta^2=0$ for $2P_0^2<P_1^2$ and

$$w^{(a)}(E_1,R_1)=0 \quad \text{for} \quad 2P_0^2\le P_1^2. \tag{2.18}$$

If we consider the case of no upper bound for the particle energy, $P_\beta<P_\alpha$ and $P_\delta=P_F$ then

$$\lim_{P_0^2\to\infty}w^{(a)}(E_1,R_1)\equiv w^{(a0)}(E_1,R_1)$$
$$=-\frac{\pi}{2}(2\pi)^{-4}\frac{2m^*(R_1)}{\hbar^2}6\left[v_0(R_1)\right]^2\frac{1}{P_1}\left\{g(P_F^2)-g(P_\gamma^2)\right\}$$
$$=-\frac{\pi}{2}(2\pi)^{-4}\frac{2m^*(R_1)}{\hbar^2}6\left[v_0(R_1)\right]^2\frac{1}{30P_1}\left\{(5P_1^2-7P_F^2)P_F^3+2(2P_F^2-P_1^2)^{\frac{5}{2}}\Theta(2P_F^2-P_1^2)\right\} \tag{2.19}$$

which agrees with the results given by [10] and [12].

B. Scattering by a particle

The process is shown by Fig. 1(b). For fixed states 1 and 2, the imaginary part of the optical potential is calculated by modifying Eq. (2.1) to fit process (b) as

$$\langle 12|w^{(b)}|12\rangle=\mathrm{Im}\lim_{\delta\to0}\frac{1}{2}\sum_{34}\frac{\langle 12|v|34\rangle n_p(3)n_p(4)\langle 43|v|21\rangle}{E_1+E_2-E_3-E_4+i\delta}. \tag{2.20}$$

The calculation of the imaginary potential in the semi-classical approximation is similar to the previous case and the result is given by

$$w^{(b)}(\mathbf{P_1R_1},\mathbf{P_2R_2})=-\frac{\pi}{2}(2\pi)^{-3}\frac{2m^*(R_1)}{\hbar^2}\frac{6}{4}\left[v_0(R_1)\right]^2\delta(\mathbf{R_1}-\mathbf{R_2})$$
$$\times\int d\mathbf{P}_3d\mathbf{P}_4\delta(\mathbf{P_1}+\mathbf{P_2}-\mathbf{P_3}-\mathbf{P_4})\delta(P_1^2+P_2^2-P_3^2-P_4^2)n_p(P_3)n_p(P_4). \tag{2.21}$$

This expression is already averaged over the spin and isospin of particle 2, so the factor $\frac{1}{4}$ appears in front of $[v_0(R_1)]^2$. Integrals over wave numbers are carried out as shown in Appendix B. For $P_0\le P_1$,

$$w^{(b)}(\mathbf{P_1R_1},\mathbf{P_2R_2})$$
$$=-\frac{\pi}{2}(2\pi)^{-3}\frac{2m^*(R_1)}{\hbar^2}\frac{6}{4}\left[v_0(R_1)\right]^2\delta(\mathbf{R_1}-\mathbf{R_2})$$
$$\times\frac{\pi}{2P}(2P_0^2-P_1^2-P_2^2)\Theta(2P_0^2-P_1^2-P_2^2), \tag{2.22}$$

where $\mathbf{P}=\mathbf{P_1}+\mathbf{P_2}$. Next the above expression is averaged over the direction of $\mathbf{P_2}$ which is carried out as shown in the previous case [see (A7)], and the following expression is obtained:

$$w^{(b)}(E_1\mathbf{R_1},\varepsilon_2\mathbf{R_2})$$
$$=-\frac{\pi}{2}(2\pi)^{-3}\frac{2m^*(R_1)}{\hbar^2}\frac{6}{4}\left[v_0(R_1)\right]^2\delta(\mathbf{R_1}-\mathbf{R_2})$$
$$\times\frac{\pi}{2P_1}(2P_0^2-P_1^2-P_2^2)\Theta(2P_0^2-P_1^2-P_2^2). \tag{2.23}$$

The only change is the replacement of P by P_1. The energy E_1 is related to P_1 by Eq. (2.4) while $\varepsilon_2 = E_2 - E_F$ is the excitation energy of particle 2 where E_2 is related to P_2 through Eq. (2.4).

The imaginary potential (2.23) still depends on the position of the participant, and we have to average over it. The probability of a particle of an excitation energy ε being at $\mathbf{R}$ is given in Thomas-Fermi theory as

$$g_p(\varepsilon, \mathbf{R}) = \frac{m^*(R)P(R)}{\pi^2\hbar^2}, \tag{2.24}$$

where $P(R)$ is the wave number determined by (2.4) for fixed E and R. Equation (2.24) is obtained from the formula given by Ring and Schuck [11]. If we integrate over position $\mathbf{R}$ then the familiar state density formula in Thomas-Fermi theory,

$$g_p(\varepsilon) = \int g_p(\varepsilon, \mathbf{R})d\mathbf{R} = \frac{4}{\pi\hbar^2}\int m^*(R)P(R)R^2dR, \tag{2.25}$$

is obtained. The final form of the imaginary potential becomes for $P_0 \leq P_1$

$$w^{(b)}(E_1, \varepsilon_2, R_1) = \frac{1}{g_p(\varepsilon_2)}\int w^{(b)}_{s_1 s_1}(E_1\mathbf{R}_1, \varepsilon_2\mathbf{R}_2)g_p(\varepsilon_2\mathbf{R}_2)d\mathbf{R}_2$$
$$= -\frac{1}{g_p(\varepsilon_2)}\frac{1}{8(2\pi)^3}\left(\frac{2m^*(R_1)}{\hbar^2}\right)^2\frac{6}{4}[v_0(R_1)]^2\frac{P_2}{P_1}(2P_0^2 - P_1^2 - P_2^2)\Theta(2P_0^2 - P_1^2 - P_2^2). \tag{2.26}$$

For $P_1 \leq P_0$ the calculation is more involved and details are given in Appendix B. For $P_F^2 + P_0^2 \leq P_1^2 + P_2^2 \leq 2P_0^2$

$$w^{(b)}(E_1\mathbf{R}_1, \varepsilon_2\mathbf{R}_2) = -\frac{\pi}{2}(2\pi)^{-3}\frac{2m^*(R_1)}{\hbar^2}\frac{6}{4}[v_0(R_1)]^2$$
$$\times\frac{\pi}{4P_1P_2}\delta(\mathbf{R}_1 - \mathbf{R}_2)\left[\frac{2}{3}P_<(3P_>^2 + P_<^2) - \frac{8}{3}(P_1^2 + P_2^2 - P_F^2)^{\frac{3}{2}}\right], \tag{2.27}$$

where $P_<$ and $P_>$ indicate the smaller and larger of P_1 and P_2, respectively.

For $2P_F^2 \leq P_1^2 + P_2^2 \leq P_F^2 + P_0^2$,

$$w^{(b)}(E_1\mathbf{R}_1\varepsilon_2\mathbf{R}_2)$$
$$= -\frac{\pi}{2}(2\pi)^{-3}\frac{2m^*(R_1)}{\hbar^2}\frac{6}{4}[v_0(R_1)]^2$$
$$\times\frac{\pi}{4P_1P_2}\delta(\mathbf{R}_1 - \mathbf{R}_2)\left[\frac{2}{3}P_<(3P_>^2 + P_<^2) - \frac{8}{3}P_F^3\right]. \tag{2.28}$$

The average over ε_1 and $\mathbf{R}_2$ is the same as before.

C. Scattering by a hole

As shown in Fig. 1(c) the procedure is the same as process (b) except for particle 2 being replaced by hole 2. The quantum mechanical expression is accordingly

$$\langle 12|w^{(c)}|12\rangle = \mathrm{Im}\lim_{\delta\to 0}\sum_{34}\frac{\langle 14|v|32\rangle n_p(3)n_h(4)\langle 23|v|41\rangle}{E_1 - E_2 - E_3 + E_4 + i\delta}, \tag{2.29}$$

and the semiclassical imaginary potential is given by

$$w^{(c)}(\mathbf{P}_1\mathbf{R}_1, \mathbf{P}_2\mathbf{R}_2) = -\pi(2\pi)^{-3}\frac{2m^*(R_1)}{\hbar^2}\frac{6}{4}[v_0(R_1)]^2\delta(\mathbf{R}_1 - \mathbf{R}_2)$$
$$\times\int d\mathbf{P}_3d\mathbf{P}_4\delta(\mathbf{P}_1 - \mathbf{P}_2 - \mathbf{P}_3 + \mathbf{P}_4)\delta(P_1^2 - P_2^2 - P_3^2 + P_4^2)n_p(P_3)n_h(P_4). \tag{2.30}$$

For $P_0^2 - P_F^2 \leq P_1^2 - P_2^2$ the integration over $\mathbf{P}_3$ and $\mathbf{P}_4$ is carried out as shown in Appendix C and the result is

$$w^{(c)}(P_1\mathbf{R}_1, P_2\mathbf{R}_2) = -\pi(2\pi)^{-3}\frac{2m^*(R_1)}{\hbar^2}\frac{6}{4}[v_0(R_1)]^2\frac{\pi}{2P}\left[(P_0^2 - P_F^2)\Theta\left(P_F - \frac{P_1^2 - P_2^2 + P^2}{2P}\right)\right.$$
$$\left.+\left\{P_0^2 - \left(\frac{P_1^2 - P_2^2 + P^2}{2P}\right)^2\right\}\Theta\left\{\frac{P_1^2 - P_2^2 + P^2}{2P} - P_F\right\}\Theta\left\{P_0 - \frac{P_1^2 - P_2^2 + P^2}{2P}\right\}\right]$$
$$\times\delta(\mathbf{R}_1 - \mathbf{R}_2). \tag{2.31}$$

After averaging over the direction of $\mathbf{P}_2$, Eq. (2.31) gives for $P_0 \leq P_1$

$$w^{(c)}(P_1\mathbf{R}_1, P_2\mathbf{R}_2) = -\pi(2\pi)^{-3}\frac{2m^*(R_1)}{\hbar^2}\frac{6}{4}[v_0(R_1)]^2\frac{\pi}{3P_1P_2}\left[(P_2^2+P_0^2-P_1^2)^{\frac{3}{2}} - (P_2^2+P_F^2-P_1^2)^{\frac{3}{2}}\Theta(P_2^2+P_F^2-P_1^2)\right] \times\Theta(P_2^2-P_1^2+P_0^2)\delta(\mathbf{R}_1-\mathbf{R}_2). \tag{2.32}$$

The average over $\mathbf{R}_2$ is same as before, and the final result is given by

$$w^{(c)}(E_1,\varepsilon_2,R_1) = -\frac{1}{g_h(\varepsilon_2)}\frac{1}{6(2\pi)^3}\left(\frac{2m^*(R_1)}{\hbar^2}\right)^2\frac{6}{4}[v_0(R_1)]^2\frac{1}{P_1} \times\left[(P_2^2+P_0^2-P_1^2)^{\frac{3}{2}} - (P_2^2+P_F^2-P_1^2)^{\frac{3}{2}}\Theta(P_2^2+P_F^2-P_1^2)\right]\Theta(P_2^2-P_1^2+P_0^2), \tag{2.33}$$

where $g_h(\varepsilon)$ is the hole state density at an energy ε.

For $P_1 \le P_0$ the imaginary potential is calculated by using Eq. (C35) but the result is not shown here because it is obtainable in just the same way as Eq. (2.33).

D. Annihilation of a particle-hole pair by a hole

For the process shown by Fig. 1(d) the quantum mechanical imaginary potential is given by

$$\langle 123|w^{(d)}|123\rangle = \mathrm{Im}\lim_{\delta\to 0}\frac{1}{2}\sum_4\frac{\langle 14|v|23\rangle n_h(4)\langle 32|v|41\rangle}{E_1-E_2-E_3-E_4+i\delta}, \tag{2.34}$$

and the semiclassical one is

$$w^{(d)}(\mathbf{P}_1\mathbf{R}_1,\mathbf{P}_2\mathbf{R}_2,\mathbf{P}_3\mathbf{R}_3) = -\pi\frac{2m^*(R_1)}{\hbar^2}\frac{6}{16}[v_0(R_1)]^2\delta(\mathbf{R}_1-\mathbf{R}_2)\delta(\mathbf{R}_1-\mathbf{R}_3) \times\int d\mathbf{P}_4\delta(\mathbf{P}_1-\mathbf{P}_2-\mathbf{P}_3+\mathbf{P}_4)\delta(P_1^2-P_2^2-P_3^2+P_4^2)n_h(P_4). \tag{2.35}$$

Averaging over directions $\mathbf{P}_2$ and $\mathbf{P}_3$ yields the following results:

$$w^{(d)}(E_1\mathbf{R}_1,E_2\mathbf{R}_2,E_3\mathbf{R}_3) = -\pi\frac{2m^*(R_1)}{\hbar^2}\frac{6}{16}[v_0(R_1)]^2\delta(\mathbf{R}_1-\mathbf{R}_2) \times\delta(\mathbf{R}_1-\mathbf{R}_3)\frac{\sqrt{P_2^2+P_3^2-P_1^2}}{4P_1P_2P_3}. \tag{2.36}$$

Averaging over E_2 and E_3, keeping $E_2+E_3=E_{23}$ as a constant, and over $\mathbf{R}_2,\mathbf{R}_3$ gives

$$w^{(d)}(E_1,\varepsilon_{23},R_1) = -\frac{1}{\omega(2h\varepsilon_{23})}\frac{\pi}{4P_1}\left(\frac{m^*(R_1)}{\pi^2\hbar^2}\right)^2\frac{6}{16} \times[v_0(R_1)]^2\sqrt{P_{23}^2-P_1^2}(2P_F^2-P_{23}^2), \tag{2.37}$$

where

$$P_{23}^2 = P_2^2+P_3^2 = \frac{2m^*(R_1)}{\hbar^2}[E_{23}-2U(R_1)], \tag{2.38a}$$

$$\varepsilon_{23} = 2E_F - E_{23}, \tag{2.38b}$$

$$\omega(2h\varepsilon_{23}) = \int g_h(\varepsilon_2)g_h(\varepsilon_{23}-\varepsilon_2)d\varepsilon_2. \tag{2.38c}$$

When the excitation energy of the participant vanishes, the imaginary potential becomes

$$w^{(d)}(E_1,0,R_1) = -\frac{\pi}{4P_1}\left(\frac{m^*(R_1)}{\pi^2\hbar^2}\right)^2\frac{6}{16}[v_0(R_1)]^2 \times\sqrt{2P_F^2-P_1^2}\frac{2m^*(R_1)}{\hbar^2}\frac{1}{g_F^2}, \tag{2.39}$$

where g_F is the single particle state density at the Fermi energy.

E. Annihilation of a particle-hole pair by a particle

The process shown by Fig. 1(e) has a contribution when $P_1 < P_0$ and vanishes if $E_0 = 0$ is assumed. The quantum mechanical imaginary potential is given by

$$\langle 123|w^{(e)}|123\rangle = \mathrm{Im}\lim_{\delta\to 0}\sum_4\frac{\langle 12|v|34\rangle n_p(4)\langle 43|v|21\rangle}{E_1+E_2-E_3-E_4+i\delta}, \tag{2.40}$$

while the semiclassical one is given by

$$w^{(e)}(\mathbf{P}_1\mathbf{R}_1,\mathbf{P}_2\mathbf{R}_2,\mathbf{P}_3\mathbf{R}_3) = -\pi\frac{2m^*(R_1)}{\hbar^2}\frac{6}{16}[v_0(R_1)]^2\delta(\mathbf{R}_1-\mathbf{R}_2)\delta(\mathbf{R}_1-\mathbf{R}_3) \times\int d\mathbf{P}_4\delta(\mathbf{P}_1+\mathbf{P}_2-\mathbf{P}_3-\mathbf{P}_4)\delta(P_1^2+P_2^2-P_3^2-P_4^2)n_p(P_4). \tag{2.41}$$

After averaging over directions $\mathbf{P}_2$ and $\mathbf{P}_3$ we obtain

$$w^{(e)}(E_1\mathbf{R}_1, E_2\mathbf{R}_2, E_3\mathbf{R}_3)$$

$$= -\pi\frac{2m^*(R_1)}{\hbar^2}\frac{6}{16}[v_0(R_1)]^2\delta(\mathbf{R}_1-\mathbf{R}_2) \times\delta(\mathbf{R}_1-\mathbf{R}_3)\frac{1}{4P_1P_2}. \quad (2.42)$$

Averaging over E_2 and E_3, keeping $E_2+E_3=E_{23}$ as a constant, and over $\mathbf{R}_2, \mathbf{R}_3$ the last equation becomes

$$w^{(e)}(E_1, \varepsilon_{23}, R_1)$$

$$= -\frac{1}{\omega(1p1h\varepsilon_{23})}\frac{\pi}{4P_1}\left(\frac{m^*(R_1)}{\pi^2\hbar^2}\right)^2 \times\frac{6}{16}[v_0(R_1)]^2\frac{2}{3}\left[\left(\frac{2m^*(R_1)}{\hbar^2}\varepsilon_{23}+P_F^2\right)^{\frac{3}{2}}-P_F^3\right], \quad (2.43)$$

where

$$\omega(1p1h\varepsilon_{23}) = \int g_p(\varepsilon_2)g_h(\varepsilon_{23}-\varepsilon_2)d\varepsilon_2. \quad (2.44)$$

For vanishing ε_{23} the above equation reduces to

$$w^{(e)}(E_1, 0, R_1) = -\frac{\pi}{4P_1}\left[\frac{m^*(R_1)}{\pi^2\hbar^2}\right]^2\frac{6}{16}[v_0(R_1)]^2 \times\frac{2m^*(R_1)}{\hbar^2}\frac{P_F}{g_F^2}. \quad (2.45)$$

F. Residual interaction and mean potential

To evaluate the imaginary potential using these formulas, the residual interaction and the mean potential must be chosen. If we employ Skyrme-type interactions, the self-consistent mean potential is obtainable with relative ease [12]. However it is rather involved to apply these interactions to the imaginary potentials for the five types of processes and we use a simplified Skyrme interaction which gives rise to nuclear saturation. The interaction is assumed to be

$$v(1,2) = (t_0+t_3\rho^\alpha)\delta(\mathbf{r}_1-\mathbf{r}_2), \quad (2.46)$$

where ρ is the nuclear density, and the parameter set which satisfies the saturation condition was given by [13] as

$$t_0 = -1020\ \text{MeV fm}^3, \quad t_3 = 2404\ \text{MeV fm}^6, \quad \alpha = 1. \quad (2.47)$$

Almost identical values have recently been used by Peilert *et al.* [14]. For the nuclear density we use the empirical one given by Bohr and Mottelson [15]

$$\rho = \rho_0(1+e^{(r-R_d)/a_d})^{-1}, \quad (2.48)$$

where ρ_0, R_d, and a_d are given by

$$\rho_0 = 0.17\ \text{fm}^{-3}, \quad R_d = (1.12A^{1/3}-0.86A^{-1/3})\ \text{fm}, \quad a_d = 0.54\ \text{fm}. \quad (2.49)$$

For the mean potential, we employ a Saxon-Woods type whose strength is linearly dependent on the energy.

$$U(r,E) = \frac{U_0+(1-\frac{m_0^*}{m})E}{1+e^{(r-R_W)/a_W}}. \quad (2.50)$$

According to Mahaux *et al.* [16] this is equivalent to using the energy-independent potential

$$\overline{U}(r) = \frac{m}{m^*(r)}\frac{U_0}{1+e^{(r-R_W)/a_W}} \quad (2.51)$$

with the effective mass

$$\frac{m^*(r)}{m} = 1-\frac{1-\frac{m_0^*}{m}}{1+e^{(r-R_W)/a_W}}, \quad (2.52)$$

where m is the nucleon mass and m_0^* is the effective mass at the nuclear center. The geometrical parameters $R_W = 1.27A^{\frac{1}{3}}$ fm and $a_W = 0.67$ fm, and the effective mass $m_0^*/m = 0.7$, are used throughout this work.

As stated before we assume symmetry with respect to neutrons and protons in the target nucleus. To be compatible with this, the depth parameter of the Woods-Saxon potential for the neutron is chosen so that the neutron particle state number is equal to the average of the observed particle state number of the neutron and proton. For protons the same potential is assumed. In Table I the single particle parameters for ^{40}Ca and ^{208}Pb are listed. The single particle numbers are taken from [16] and the depth parameter U_0 is fixed by using the geometrical parameters R_W and a_W. For this mean potential, the Fermi energy E_F and the state density (for neutrons and protons) at this energy g_F are also listed.

Between two magic nuclei ^{40}Ca and ^{208}Pb, we choose ^{93}Nb because much experimental data and theoretical analyses are available. For this nucleus, the depth parameter is fixed assuming a linear function of the neutron excess. By fitting with the data for two magic nuclei it becomes

$$U_0 = -45.51+17.68(N-Z)/A\ \text{MeV}. \quad (2.53)$$

The obtained value is given in Table I, where the rate

TABLE I. Potential depth parameter U_0, Fermi energy E_F, single particle state density at E_F, derivatives of these two quantities with respect to U_0 for nuclei used in this work. For ^{40}Ca 20 neutron particle states and 8 proton particle states are assumed, while 58 and 44 states for ^{208}Pb.

	^{40}Ca	^{208}Pb	^{93}Nb
U_0 (MeV)	−45.51	−41.77	−43.42
E_F (MeV)	−10.06	−9.27	−9.57
g_F (MeV^{-1})	2.04	9.04	4.32
$\frac{dE_F}{dU_0}$	0.87	1.05	0.96
$\frac{dg_F}{dU_0}$	0.038	0.148	0.078

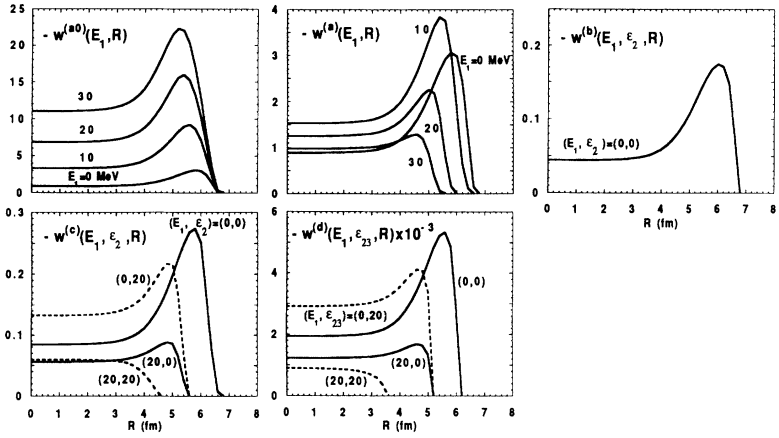

FIG. 2. R-dependence of elementary process imaginary potentials in units of MeV for ^{93}Nb. Curves are plotted for ($a0$) and (a) processes varying the incident energy, while for other processes by varying both the incident energy and the excitation energy of the participant.

of change of Fermi energy and the rate of change of the state density with the depth parameter are also shown to see the effect of a change of U_0.

G. Results of calculation

In Fig. 2, the R dependence of the imaginary potential for $w^{(a0)}(E,R)$, which corresponds to $E_0 = \infty$, and those for the other four kinds of elementary processes corresponding to $E_0 = 0$ are shown. For process (a) the incident energy E_1 varies, while for (b)–(d) both E_1 and the excitation energy of the participant ε vary. Process (e) is not shown because it vanishes for $0 = E_0 \leq E_1$. Except for the highest excitation energy of the participant, the R dependence is surface peaked, which is supposed to be caused by the R dependence of the effective mass and the density-dependent effective interaction, but details are a little different for each case. Results for ^{93}Nb are shown, but those for ^{40}Ca and ^{208}Pb have similar behavior.

The energy dependence of the imaginary potential of the elementary processes at the nuclear center is shown in Fig. 3. While $w^{(a0)}$ increases with energy approximately like $(E - E_F)^2$, which is the well-known behavior due to the increase of the state density of intermediate states, $w^{(a)}$ increases up to 7 MeV but then decreases almost linearly and vanishes as shown by (2.18). This is of course due to the restriction of particle states to the Q space. For $w^{(b)}, w^{(c)}$, and $w^{(d)}$ the strength for several energies E_1 of the incident nucleon are shown as a function of the excitation energy ε_2 of the participant. This dependence on ε_2 is weak except for $w^{(b)}$. The magnitudes of $w^{(b)}$ and $w^{(c)}$ are one order smaller than $w^{(a)}$and $w^{(d)}$ is two orders smaller than $w^{(a)}$.

So far the imaginary part of the optical potentials has been evaluated using (2.1) for process (a) and similar expressions for other processes as explained in this section. However, they are also expressed as

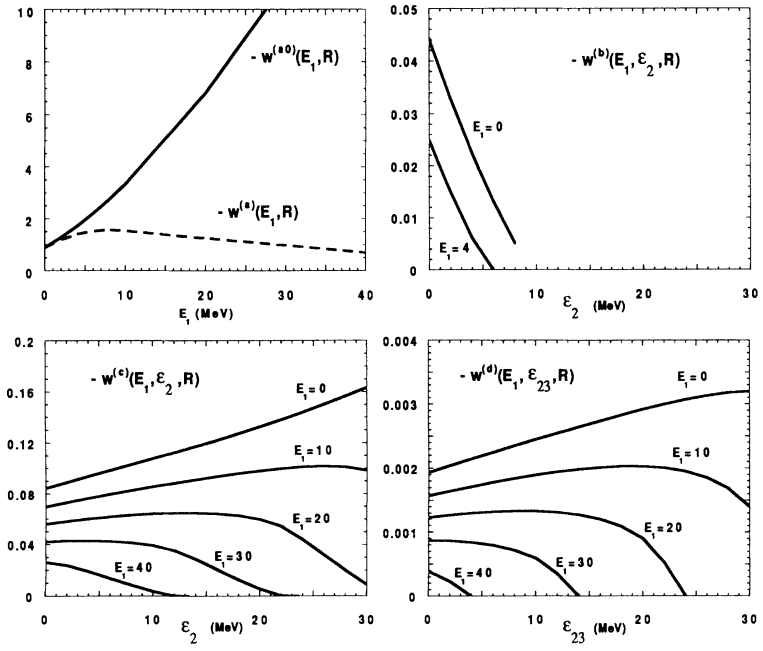

FIG. 3. Energy dependence of elementary process imaginary potentials in units of MeV for ^{93}Nb. The imaginary potential at the nuclear center $R = 0$ is plotted for processes ($a0$) and (a) against the incident energy, while for other processes against the excitation energy of the participant by varying the incident energy.

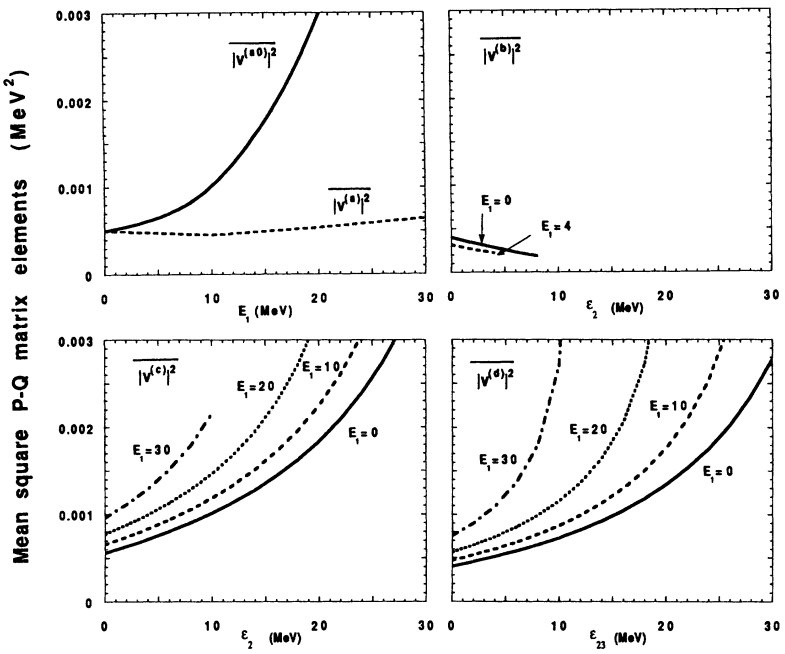

FIG. 4. Mean square P-Q matrix elements in units of MeV^2 as a function of energies for ^{93}Nb. Each curve in this figure corresponds related one in Fig. 3.

$$w^{(i)}(E_1,\varepsilon_2) = \pi\overline{|v^{(i)}|^2}(E_1,\varepsilon_2)\omega_i(\varepsilon), \qquad (2.54)$$

where $i = a,\ldots,d$ and $\overline{|v^{(i)}|^2}$ is the average square of matrix elements between P and Q spaces corresponding to the process (i). The next factor $\omega_i(\varepsilon)$ is the state density of intermediate states with the excitation energy $\varepsilon = E_1 - E_F + \varepsilon_2$.

We evaluate the average square matrix elements for the four types of processes by using the imaginary potential obtained here and the state density evaluated by the Thomas-Fermi theory. For process (a) a particle-hole pair of neutrons or protons is created, and the state density for neutrons and protons must be used. In other processes, the isospins of intermediate states are all fixed once the initial state is fixed. Therefore the state density for neutrons (or protons) should be used. The results are shown in Fig. 4. For process (a) the average square matrix element is a function of E_1 and the dependence on this is weak. For other processes they depend on E_1 as well as ε_2, so they are plotted against the latter for each value of the former. Except for process (b), they increase with E_1 as well as ε_2. As shown in the next section, the important part of the imaginary potential is near $\varepsilon_2 \approx 0$ and we see that the four types of processes have almost equal values. It is shown that the average square matrix elements for the four processes are the same in the limit of zero excitation energy for all participating particles and holes.

In Fig. 5 the mean square matrix elements for van-

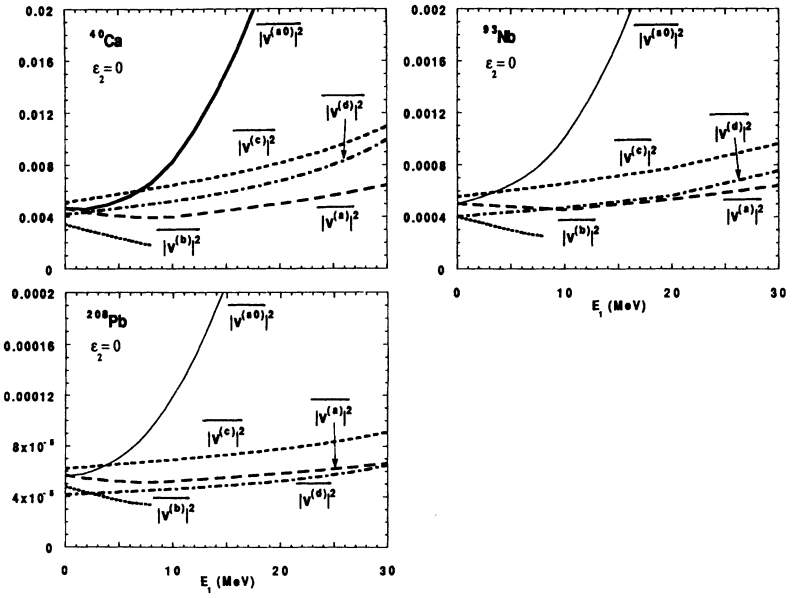

FIG. 5. Mean square P-Q matrix elements in units of MeV^2 as functions of E_1 for fixed $\varepsilon_2 = 0$ for ^{40}Ca, ^{93}Nb, and ^{208}Pb.

ishing excitation energy of the participant are plotted against E_1 for three nuclei, and they show similar behavior. Except for process $(a0)$, which shows rapid increases with energy, the energy and type dependences are weak. However, the absolute magnitude decreases as A increases.

Herman *et al.* [7] assumed in their calculation of MSC that the average square of matrix elements are the same for all types of processes. Our calculation justifies their assumption. But they used the conventional imaginary potentials $w^{(a0)}$, which overestimates the transmission coefficients.

III. GENERAL CASE

The imaginary part of the optical potential in the general case is obtained from those for the elementary processes by taking account of the spectator. The target nucleus is assumed to be an n_p-particle and n_h-hole state with the excitation energy ε. First we consider process (a) with $\Delta m = 2$. In this case the spectator has nothing to do with the imaginary part if we neglect the Pauli blocking effect, and the imaginary potential of the elementary process is equal to that of the whole system:

$$W^{(a)}(n_p, n_h, E, \varepsilon, R) = w^{(a)}(E, R). \tag{3.1}$$

For other processes, the imaginary potential of the elementary processes is averaged over the energy of the particle or hole with which the incident particle interacts. It is convenient to introduce the probability function $P(n_p n_h \varepsilon; n_{p_1} n_{h_1} \varepsilon_1)$ for a nucleus with an n_p-particle and n_h-hole excitation at an energy ε having a part with an n_{p_1}-particle and n_{h_1}-hole at an energy ε_1. Neglecting the Pauli blocking effect this quantity is given by

$$P(n_p n_h \varepsilon; n_{p_1} n_{h_1} \varepsilon_1) = \frac{\omega(n_{p_1}, n_{h_1}, \varepsilon_1)\omega(n_p - n_{p_1}, n_h - n_{h_1}, \varepsilon - \varepsilon_1)}{\binom{n_p}{n_{p_1}}\binom{n_h}{n_{h_1}}\omega(n_p n_h \varepsilon)} \tag{3.2}$$

where the binomial coefficients are to correct for double counting. If this probability function is integrated over ε_1 then we obtain unity.

As the imaginary potential of the elementary process is calculated based on the Thomas-Fermi theory, the state density should be based on the same theory. However, its calculation is complicated and, for reasons which will soon becomes clear, the much simpler Obložinský formula based on the equidistant single particle level [17] is adopted. It is given by

$$\omega(n_p, n_h, \varepsilon) = \frac{g^{(n_p+n_h)}}{n_p! n_h! (n_p + n_h - 1)!} \sum_{i=0}^{n_p} \sum_{j=0}^{n_h} (-1)^{(i+j)} \binom{n_p}{i} \binom{n_h}{j} \times \Theta(\varepsilon - \alpha_{n_p n_h} - i\varepsilon_{p\max} - j\varepsilon_{h\max})(\varepsilon - A_{n_p n_h} - i\varepsilon_{p\max} - j\varepsilon_{h\max})^{n_p+n_h-1}, \tag{3.3}$$

where $\varepsilon_{p\max} = E_0 - E_F$ is the maximum excitation energy of particles, and $\varepsilon_{h\max}$ is that of holes. A constant single particle state density g is assumed and the Pauli effect is included by the two correction factors $\alpha_{n_p n_h}$ and $A_{n_p n_h}$, which will be neglected in the following calculations.

Before using the approximate formula (3.3) we compare the two predictions for the cases to be used in evaluating the imaginary potential. In Fig. 6, particle, hole,

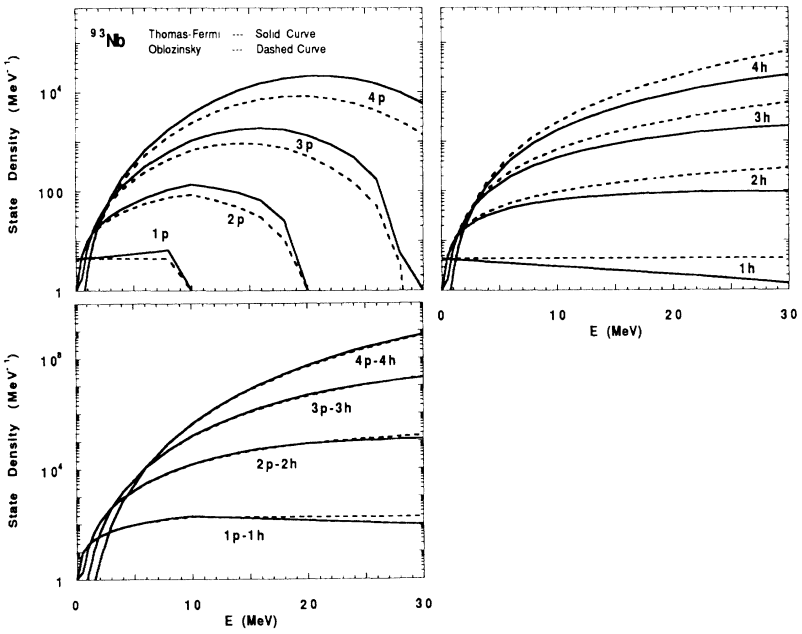

FIG. 6. State densities for particle, hole and particle-hole states in ^{93}Nb. Solid curves represent those calculated by Thomas-Fermi model, and dashed curves represent results calculated with equidistant model.

and particle-hole state densities for ^{93}Nb are shown. In the case of particles, the approximate formula underestimates because the single particle state density increases as the excitation energy increases. For the case of holes, the tendency is opposite. In the particle-hole case, the differences are smaller compared with the previous two cases, as the two effects mostly cancel.

In Fig. 7 we show the probability function given by (3.2) for the cases to be used in our calculations as functions of participant energy ε_1. Figure 7(a) represents typical cases of high exciton numbers, while Fig. 7(b) corresponds to low exciton numbers. The sharp peaks at low energy observed in Fig. 7(a) are interpreted as follows. The probability (3.2) is proportional to a product of two state densities. For the cases of $n_{p_1} + n_{h_1} = 1$, to which processes (b) and (c) correspond, the first state density on the right-hand side of Eq. (3.2) is a constant. The energy dependence comes from the second state density, and it is approximately given by

$$P(n_p n_h \varepsilon; 10\varepsilon_1) = P(n_p n_h \varepsilon; 01\varepsilon_1) = \frac{n_p + n_h - 1}{\varepsilon}\left(1 - \frac{\varepsilon_1}{\varepsilon}\right)^{n_p+n_h-2}, \quad (3.4)$$

whose half-width is given by

$$\Delta\varepsilon_1 \approx \varepsilon \ln 2/(n_p + n_h - 2). \quad (3.5)$$

For the process (d) $n_{p_1} = 0$ and $n_{h_1} = 2$ and the probability function has a sharp peak, which is approximately expressed by

$$P(n_p n_h \varepsilon; 02\varepsilon_1) \approx \frac{n_p + n_h - 1}{\varepsilon}\left(1 - \frac{1}{n_p + n_h - 2}\right)^{n_p+n_h-3} \times \exp\left[-\frac{1}{2}\left(\frac{\varepsilon_1 - \varepsilon_1^0}{\varepsilon_1^0}\right)^2\right]. \quad (3.6)$$

The peak energy is given by

$$\varepsilon_1^0 = \frac{\varepsilon}{n_p + n_h - 2} \quad (3.7)$$

and the half-width is

$$\Delta\varepsilon_1^0 = \varepsilon_1^0\sqrt{2\ln 2}. \quad (3.8)$$

These formulas are derived just taking the $i = j = 0$ term of the state density formula (3.3), and assuming $n_p + n_h \gg 1$. When these conditions are not valid a broad distribution is seen as in Fig. 7(b). It is also noted that the probability function given by (3.2) is independent of the single particle state density as we use the equidistant state density formula (3.3).

The imaginary potentials in general cases for processes (b), (c), and (d) are calculated using the imaginary potential for elementary processes and the probability functions as

$$W^{(b)}(n_p n_h, E, \varepsilon, R) = n_p \int w^{(b)}(E, \varepsilon_1, R) \times P(n_p n_h \varepsilon, 1, 0, \varepsilon_1) d\varepsilon_1, \quad (3.9a)$$

$$W^{(c)}(n_p n_h, E, \varepsilon, R) = n_h \int w^{(c)}(E, \varepsilon_1, R) \times P(n_p n_h \varepsilon, 0, 1, \varepsilon_1) d\varepsilon_1, \quad (3.9b)$$

$$W^{(d)}(n_p n_h, E, \varepsilon, R) = \frac{n_h(n_h - 1)}{2} \int w^{(d)}(E, \varepsilon_1, R) \times P(n_p n_h, \varepsilon, 0, 2, \varepsilon_1) d\varepsilon_1. \quad (3.9c)$$

We have evaluated the imaginary potential using the above formulas for the case of ^{93}Nb. The R dependence is shown in Figs. 8 and 9, and it is similar to that of elementary processes. The imaginary potential is calculated for target excitation energies $\varepsilon = 0, 10$, and 20 MeV, and low exciton states $0p$-$0h$, $1p$-$1h$, and $2p$-$2h$, which are important in absorption processes. For convenience the ground state is considered as the $0p$-$0h$ state. In Fig. 8 the curves for $\varepsilon = 0, 10$, and 20 MeV coincide with each other inside the nucleus, but split away at the nuclear surface. The spread increases as the excitation energy increases. In Fig. 9 the R dependence for higher exciton states is shown taking process (c) as an example. The excitation energy dependence becomes weak as the exciton number increases, and the magnitude is clearly shown to be proportional to n_p. For process (d) it is proportional to $n_h(n_h - 1)/2$. These dependences are easily understood as the probability function (3.2) has a sharp peak near $\varepsilon_1 = 0$, while the dependence of elementary processes on ε_1 is weak.

In Fig. 10 the incident energy dependence of the central part of the imaginary potential is shown. It is clearly seen that the excitation energy dependence is weak as

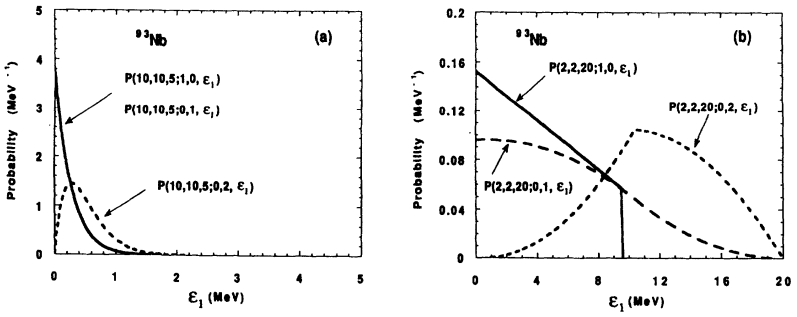

FIG. 7. The probability function $P(n_p n_h \varepsilon; n_{p_1} n_{h_1} \varepsilon_1)$ which represents the probability of finding a n_{p_1}-particle and n_{h_1}-hole state of excitation energy ε_1 in a n_p-particle and n_h-hole state of excitation energy ε in ^{93}Nb.

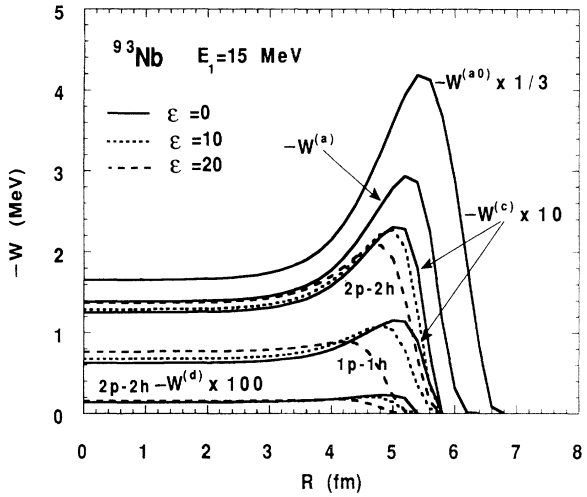

FIG. 8. R dependence of imaginary potentials for E_1 =15 MeV and $\varepsilon = 0$, 10, and 20 MeV. The target nucleus is ^{93}Nb of low exciton number $1p$-$1h$ and $2p$-$2h$ states. Note different multiplying factors for different processes.

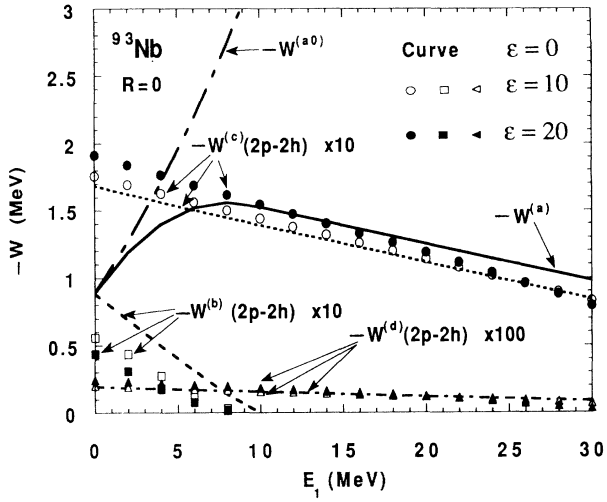

FIG. 10. Energy dependence of imaginary potentials at the nuclear center for target nucleus ^{93}Nb of $2p$-$2h$ states with excitation energies $\varepsilon = 0, 10$, and 20 MeV.

the incident energy E_1 increases.

Considering these dependences shown in Figs. 8–10 it is a good approximation to replace the probability function by $\delta(\varepsilon_1)$. Equations (3.9) become

$$W^{(b)}(n_p n_h, E, \varepsilon, R) = n_p w^{(b)}(E, 0, R), \tag{3.10a}$$

$$W^{(c)}(n_p n_h, E, \varepsilon, R) = n_h w^{(c)}(E, 0, R), \tag{3.10b}$$

$$W^{(d)}(n_p n_h, E, \varepsilon, R) = \frac{n_h(n_h - 1)}{2} w^{(d)}(E, 0, R), \tag{3.10c}$$

where $w^{(b)}$ and $w^{(c)}$ are easily obtained from (2.26) and (2.33). For the last equation $w^{(d)}$ is given by (2.39).

For emission from low exciton states the process with $\Delta m = -2$ is also important, because the final state density is the largest among the four processes. In such cases the nuclear surface part of the imaginary potential is important, and the original formulas (3.9) should be used. For absorption processes the dominant one is (a) and the contributions from other processes are small, so the approximate formulas (3.10) may be enough. However, it is necessary to evaluate the transmission coefficient to see how much the approximate formulas (3.10) are useful in exceptional cases.

The same formulas may be applicable in the case of internal transition. These make the calculation of the parameters used in preequilibrium processes much easier than the original Feshbach *et al.* [2] formulation.

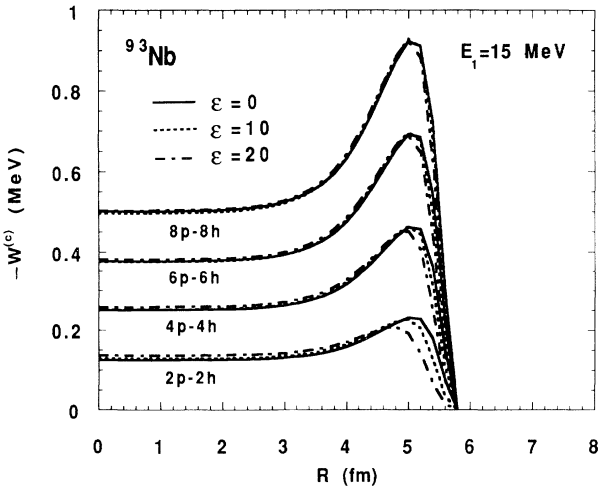

FIG. 9. R dependence of imaginary potentials $W^{(c)}(E_1, \varepsilon)$ for E_1 = 15 MeV, $\varepsilon = 0, 10$, and 20 MeV, and target nucleus ^{93}Nb of $n_p = n_h = 2, 4, 6$, and 8 states.

IV. TRANSMISSION COEFFICIENT

In preequilibrium theories, formation and decay rates of the compound system is obtained from transmission coefficients, which are usually calculated using the matrix elements between P and Q space. The transmission coefficient for the channel a to form compound states with the exciton number m is given by [5,7]:

$$T_{am} = \frac{4\pi^2 \overline{|v_{m,a}|^2} \omega_m}{(1 + \pi^2 \overline{|v_{m,a}|^2} \omega_m)^2}, \tag{4.1}$$

where the quantity $\pi \overline{|v_{m,a}|^2} \omega_m$ corresponds to the imaginary part of the optical potential which appeared in (2.54). However, our approach is to calculate the transmission coefficients quantum mechanically using the imaginary potential obtained semiclassically. In the following the general formulation for calculating the transmission coefficients is outlined. The relation with the formula (4.1) will be discussed later.

The Schrödinger equation for the whole system is given by

$$(H_0 + H_t + V - E_a)\Psi_a^{(+)} = 0, \tag{4.2}$$

in which a indicates the incident channel, H_t the Hamiltonian for the target nucleus, and V the residual interaction between the particle and the target nucleus. The particle Hamiltonian is written as

$$H_0 = K + U + iW, \tag{4.3}$$

where K represents the kinetic energy, U the real part of the optical potential, and W is the imaginary part. The zeroth-order equation with respect to V is

$$(H_0 + H_t - E_a)\Phi_a^{(+)} = 0. \tag{4.4}$$

Both wave functions $\Psi_a^{(+)}$ and $\Phi_a^{(+)}$ are eigenfunctions of non-Hermitian Hamiltonians, so they do not make orthogonal sets and are normalized as

$$\lim_{W\to 0}\langle\Psi_a^{(+)}|\Psi_b^{(+)}\rangle = \lim_{W\to 0}\langle\Phi_a^{(+)}|\Phi_b^{(+)}\rangle = \delta_{ab}\delta(E_a - E_b). \tag{4.5}$$

These two wave functions are connected by the relation

$$\Psi_a^{(+)} = \Phi_a^{(+)} + \frac{1}{E - H_0 - H_t - V}V\Phi_a^{(+)}. \tag{4.6}$$

The general transmission matrix is given by [18]

$$T_{abm} = -4\pi\langle\Psi_a^{(+)}|W_m|\Psi_b^{(+)}\rangle. \tag{4.7}$$

The imaginary part of the optical potential is given quantum mechanically by

$$W_m = -\pi H_{PQ}Q_m\delta(E - H_{QQ})Q_m H_{QP}, \tag{4.8}$$

which contains the projection operator Q_m onto m-exciton states.

We now evaluate the transmission coefficient in the perturbation approximation with respect to V [19]. We assume the independent particle model for the target nucleus, so H_t is a sum of single particle Hamiltonians. Then the exciton number of the target nucleus and consequently that of the channel a may be fixed, which is denoted by ν_a. The zeroth-order transmission coefficient is given by

$$T_{aam}^{(0)} = -4\pi\langle\Phi_a^{(+)}|W_m|\Phi_a^{(+)}\rangle, \tag{4.9}$$

while the second-order one is given by

$$T_{aan}^{(2)} = -4\pi\langle\Phi_a^{(+)}|VG_0^{\dagger}W_nG_0V|\Phi_a^{(+)}\rangle, \tag{4.10}$$

and

$$G_0 = \frac{1}{E - H_0 - H_t} \tag{4.11}$$

is the zeroth-order Green's function.

Here we employ the imaginary potentials obtained in the previous section. They are calculated for the target state specified by the particle and hole numbers n_p and n_h. Then the exciton number for the initial channel is given by $\nu_a = m_0 = n_p + 1 + n_h$. Intermediate states in the Q space have one of the exciton numbers $m = m_0, m_0 \pm 2$. The corresponding imaginary potentials $W_{m_0\to m}(r)$ are more explicitly written as

$$W_{m_0\to m_0+2}(r) = W^{(a)}(n_pn_hE\varepsilon r), \tag{4.12a}$$

$$W_{m_0\to m_0}(r) = W^{(b)}(n_pn_hE\varepsilon r) + W^{(c)}(n_pn_hE\varepsilon r), \tag{4.12b}$$

$$W_{m_0\to m_0-2}(r) = W^{(d)}(n_pn_hE\varepsilon r). \tag{4.12c}$$

The imaginary potential appearing in (4.3) is given by

$$W_{m_0}(r) = \sum_m W_{m_0\to m}(r). \tag{4.13}$$

The channel wave function specified by a channel index a is written as a product of the particle wave function

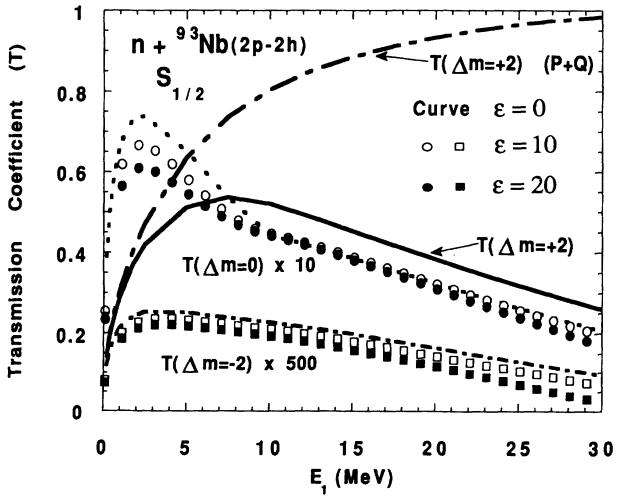

FIG. 11. Transmission coefficients for $s_{1/2}$ neutron to ^{93}Nb $2p$-$2h$ states as a function of E_1 with $\varepsilon = 0, 10$, and 20 MeV.

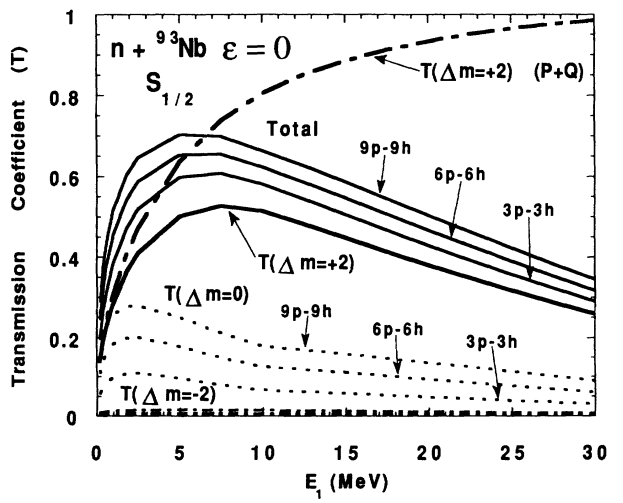

FIG. 12. Transmission coefficients for $s_{1/2}$ neutron to ^{93}Nb $n_p = n_h = 3, 6$, and 9 states as a function of E_1 with $\varepsilon = 0$.

specified by $p_a = (t_{z_a}, l_a, j_a)$ and the target nucleus one specified by $\lambda_a = (\nu_a - 1, I_a)$;

$$\Phi_a^{(+)} = \left[\phi_{p_a}^{(+)} \varphi_{\lambda_a}\right]_{\nu_a, J_a M_a}, \tag{4.14}$$

$$\phi_{p_a}^{(+)} = \frac{1}{r} u_{t_{z_a} l_a j_a}^{(+)} \chi_{l_a j_a m_a}, \tag{4.15}$$

where ν_a is the exciton number and $J_a M_a$ are the total angular momentum and its z component of the channel a. It is not necessary to explain the other quantum numbers. The single particle wave function satisfies the equation

$$[K + U + iW_{m_0}(r) - E]\phi_{p_a}^{(+)} = 0. \tag{4.16}$$

Using these notations the zeroth-order transmission coefficient is given by

$$T_{aam}^{(0)} = 4\pi \int_0^\infty |u_{p_a}^{(+)}(r)|^2 \left[-W_{\nu_a \to m}(r)\right] dr, \tag{4.17}$$

with $|\nu_a - m| = 2, 0$.

The zeroth-order transmission coefficients are calculated for the neutron scattering by ^{93}Nb of $2p$-$2h$ states and the results are shown in Fig. 11 for the $s_{1/2}$ neutron. The full line shows the transmission coefficient for $\Delta m = 2$ with $E_0 = 0$, while the dot-dashed curve shows results for the same process but taking $E_0 = \infty$, which is labeled as $P + Q$ (absorption). The two curves coincide at low energy, but deviate with increasing energy. The full curve corresponding to Q absorption has its peak around 7 MeV and falls off with energy. However, the difference between the two curves is not so much as for those of the imaginary potential because the transmission coefficient cannot exceed unity. In the figure, the transmission coefficients for $\Delta m = 0$ and -2 are also shown to indicate the excitation energy dependence. If the approximation (3.10) is good, there should be no dependence within each group. However, the case shown here corresponds to the situation shown by Fig. 7(b), and some dependence appears at the low energy part of the $\Delta m = 0$ case. Otherwise the dependence is weak and may be ignored.

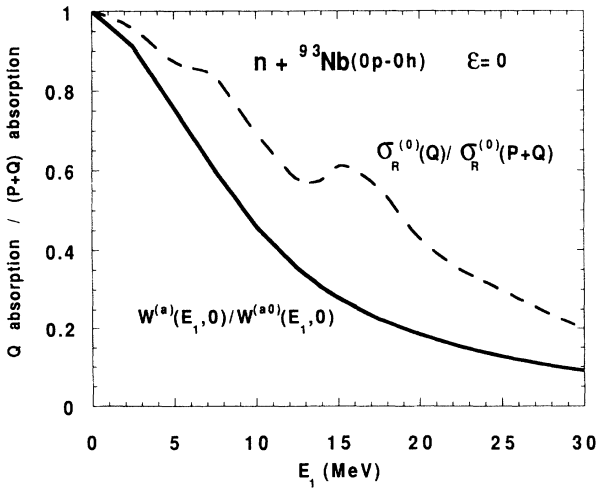

FIG. 13. Ratio of reaction cross sections for Q absorption to $P + Q$ absorption $\sigma_R^{(0)}(Q)/\sigma_R^{(0)}(P + Q)$ is shown by a dotted line for neutron scattering by ^{93}Nb. For comparison, that of imaginary potentials at the nuclear center $W^{(a)}(E_1, 0)/W^{(a0)}(E_1, 0)$ is also shown by a full line.

In Fig. 12 the exciton number dependence is shown for the same cases as for the previous figure except that the target excitation energy is kept to zero while the exciton number is changed. Apparently the exciton number dependence of the imaginary potential is reproduced in the transmission coefficients. This indicates that the approximation of (3.10) is good while the transmission coefficient is far less than the unitary limit.

Data shown in the figures are with respect to one partial wave only. To see the effect of all partial waves, the reaction cross section is calculated by

$$\sigma_R = \frac{\pi}{2k_a^2} \sum_{lj} (2j + 1) T_{lj}, \tag{4.18}$$

where T_{lj} is the transmission coefficient for the partial wave with orbital and total angular momenta l and j, respectively. For the same reaction as in Figs. 11 and 12 but keeping both the exciton number and the excitation energy to zero, the ratio of reaction cross sections corresponding to Q to $P + Q$ absorption is shown in Fig. 13. The curve shows the general tendency of being a decreasing function of the incident energy. There appears a small bump for which we do not have clear explanation, but it may be due to competition between an increase in the effective number of partial waves and a decrease in the magnitude of the imaginary potential with energy. In the figure the ratio of imaginary parts is also shown and the decreasing tendency is stronger than for the ratio of transmission coefficients. This is due to the saturation property of the transmission coefficient by unitarity.

We now evaluate the second-order transmission coefficient for the ground-state target ($0p$-$0h$). After the first collision the intermediate state becomes a $2p$-$1h$ state with one nucleon in the continuum. This state decays to form a $3p$-$2h$ state by the imaginary potential $W^{(a)}$. This is the main process and other processes are not considered here. As for the channel wave function for the intermediate state c, the target nuclear state λ_c is assumed to be a $1p$-$1h$ state and is given by

$$\varphi_{\lambda_c} = [\phi_h \phi_p]_{I_c M_c}, \tag{4.19}$$

where a particle p and a hole h are coupled to the angular momentum I_c and its z component M_c. First, the matrix element of the interaction which appeared in (4.10) is expressed as

$$\langle [\varphi_{\lambda_c} \chi_{j_c}]_{j_a m_a} | V | \Phi_a^{(+)} \rangle$$

$$= \sum \langle j_h m_h j_p m_p | I_c M_c \rangle \langle I_c M_c j_c m_c | j_a m_a \rangle$$

$$\times \langle \phi_p \chi_{j_c m_c} | V | \phi_{\bar{h}} \phi_a^{(+)} \rangle_A. \tag{4.20}$$

The calculation of the matrix element is straightforward, and the result is given by

$$\langle[\phi_{\lambda_c}\chi_{j_c}]_{j_a m_a}|V|\Phi_a^{(+)}\rangle = r^{-3}u_p^*(r)v_0(r)u_h^*(r)u_a^{(+)}(r) \times\frac{(-1)^{j_h+j_p}}{\sqrt{(2I_c+1)(2j_a+1)}}V_{pcha}^{I_c}, \tag{4.21}$$

where

$$V_{pcha}^{I_c} = \langle j_p\|Y_{I_c}\|j_h\rangle\langle j_c\|Y_{I_c}\|j_a\rangle -\delta_{t_z(h),t_z(a)}\langle j_p\|Y_{I_c}\|j_a\rangle\langle j_c\|Y_{I_c}\|j_h\rangle. \tag{4.22}$$

The second term of the right-hand side of (4.22) is for antisymmetrization of like nucleons. The reduced matrix element is given in terms of the Clebsch-Gordan coefficient by

$$\langle j\|Y_I\|j'\rangle = (-1)^{j'-1/2}\sqrt{\frac{(2j+1)(2j'+1)}{4\pi}} \times\langle j\tfrac{1}{2}j'-\tfrac{1}{2}|I0\rangle\frac{1+(-1)^{l+l'+I}}{2}, \tag{4.23}$$

where l indicates the orbital angular momentum of the orbit j.

The Green's function is given by

$$\langle r|\frac{1}{E-K-U-iW}|r'\rangle = -\sum_{jl}\sqrt{\frac{\pi k}{E}}O(r_>)u^{(+)}(r_<) \times\sum_{\mu}|\chi_{ljm}\rangle\langle\chi_{ljm}|, \tag{4.24}$$

where $r_>$ and $r_<$ represent the larger and smaller among r and r', respectively, and $O(r)$ is the radial part of the outgoing wave solution of (4.4) and its asymptotic form is

$$O(r) = I^*(r) \sim \exp\left[i\left(kr-\eta\ln(2kr)-\frac{\pi}{2}l+\sigma_l\right)\right], \tag{4.25}$$

where η and σ_l are the Coulomb parameter and the Coulomb phase shift. The asymptotic form of $u^{(+)}(r)$ is

$$u_a^{(+)}(r) \sim \frac{i}{\hbar}\sqrt{\frac{m}{2\pi k}}\left[I(r)-S_{aa}^{(0)}O(r)\right], \tag{4.26}$$

where $S_{aa}^{(0)}$ is the zeroth-order S matrix. Using (4.24) and (4.22) the second-order transmission coefficient (4.10) is calculated as

$$T_{aan}^{(2)} = \sum_{cphI_c}\frac{4\pi^2k_c}{E_c}\frac{(V_{pcha}^{I_c})^2}{(2I_c+1)(2j_a+1)} \times\int_0^\infty|f_{pcha}(r)|^2\left[-W_n(r)\right]dr, \tag{4.27}$$

where

$$f_{pcha}(r) = O_c(r)\int_0^r u_p^*(r')u_c^{(+)}(r')v_0(r')u_h^*(r')u_a^{(+)}(r')\frac{dr'}{r'^2} +u_c^{(+)}(r)\int_r^\infty u_p^*(r')O_c(r')v_0(r')u_h^*(r')u_a^{(+)}(r')\frac{dr'}{r'^2}. \tag{4.28}$$

The second-order transmission coefficient is evaluated for ^{40}Ca and ^{208}Pb with incident neutrons. The magnitude of the second order is more or less the same as that of the zeroth order, but in some partial waves the transmission coefficient exceeds unity in contradiction with unitarity. This shows the breakdown of the perturbation approximation. The second-order transmission coefficient is a sum of many intermediate components, whose number exceeds a thousand in the case of ^{208}Pb. Although each component is very small, the sum becomes as large as 2.

Despite the violation of unitarity the reaction cross section is calculated and shown in Fig. 14 for n+^{208}Pb. The second-order reaction cross section is shown by the dotted curve and the zeroth-order Q-space absorption by the solid curve, both in units of the zeroth-order $P+Q$ absorption cross section at the corresponding energy. The second-order cross section starts around 4 MeV, increases with energy exceeding the zeroth-order cross section at 9 MeV, has its peak around 17 MeV, and thereafter decreases. This behavior is considered qualitatively correct although not quantitatively. As a consequence of the limitation of absorption to Q space, the reaction cross section decreases from a certain energy, while the second-order contribution increases fast to reach the peak, and then decreases gradually.

We return to Eq. (4.1) and show that it is derived from (4.17) with an approximation. The radial wave function $u^{(+)}(r)$ satisfies

$$(K_r+U+iW-E)u^{(+)}(r) = 0, \tag{4.29}$$

where K_r represents the kinetic energy in terms of the

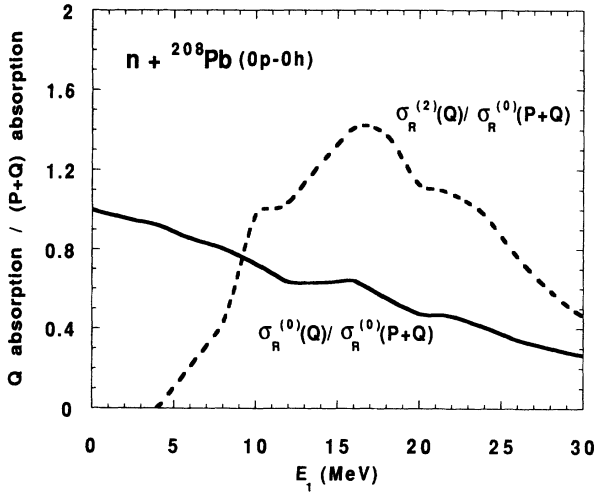

FIG. 14. Ratio of the second-order reaction cross section to the zeroth-order $P+Q$ absorption cross section of neutron for ^{208}Pb is shown by a dotted line as a function of the incident energy. The final states are $3p$-$2h$ states. The zeroth-order reaction cross section ratio $\sigma_R^{(0)}(Q)/\sigma_R^{(0)}(P+Q)$ is also shown by a solid line for comparison.

radial coordinate. Between the radial wave function $u^{(+)}$ for the optical potential and $u^{R(+)}$ for the real part of the optical potential, the following relation analogous to Eq. (4.6) holds,

$$u^{(+)}(r) = \left(1 + \frac{1}{E - K_r - U - iW} iW\right) u^{R(+)}(r). \tag{4.30}$$

The Green's function in Eq. (4.30) is evaluated by expanding in terms of iW. Neglecting the principal part of the zeroth-order Green's function

$$\frac{1}{E^+ - K_r - U} \approx -i\pi\delta(E - K_r - U), \tag{4.31}$$

the transmission coefficient becomes

$$T^{(0)}_{am} = \frac{4\pi\langle u_a^{R(+)}|(-W)|u_a^{R(+)}\rangle}{\left[1 + \pi\langle u_a^{R(+)}|(-W)|u_a^{R(+)}\rangle\right]^2}, \tag{4.32}$$

which is equal to (4.1) if the relation between the imaginary part of the optical potential and the matrix element between Q and P spaces is considered. We tested the approximation (4.32) in the case of the calculations shown in Fig. 2, and found that differences between (4.17) and (4.32) were at most 10%.

V. SUMMARY AND DISCUSSION

We have shown that a delta-function-type residual interaction combined with the Thomas-Fermi approximation gives rise to simple formulas for the imaginary parts of the optical potential for fixed exciton number to be used in preequilibrium reactions. The effect of spectators is taken into account by the aid of the probability function, which may be approximated by $\delta(\varepsilon_2)$ in most cases. Calculations of the transmission coefficient are straightforward. Therefore our formulation is much simpler than that of Feshbach *et al.* [2], which is widely used in data analyses. To use our imaginary potential in phenomenological analyses, finer adjustment of parameters may be necessary.

By using a simple model we have also calculated the second-order transmission coefficients, where the incident nucleon makes a collision in P space to create a particle-hole pair before it is captured. The second-order transmission coefficients are found to be of the same order as the zeroth-order ones, and are important in preequilibrium analyses. For quantitative estimation of this effect more elaborate calculations are necessary, as our second-order coefficients exceed the unitarity limit in some cases.

We have used a simplified version of the Skyrme interaction to avoid complicated calculation, but it is interesting to compare the results with the full version. Zhuo *et al.* [12] performed such a calculation for $P + Q$ absorption, which is shown by the curve denoted as "Zhuo $(P + Q)$" in Fig. 15. To obtain the imaginary potential with the full version, we use the same formula as Zhuo *et al.* for $W^{(a0)}$ and the similar formula for $W^{(a)}$ which satisfies the condition that the intermediate states are restricted to Q space. The Skyrme interaction GS2, which was used by Zhuo *et al.*, is employed to calculate $W^{(a0)}$ and $W^{(a)}$ with the method explained in Sec. II, namely, the relation (2.4) and effective mass (2.52). The results, together with our results with the simplified Skyrme interaction (2.46) and (2.47), are shown in Fig. 15 for 20 MeV neutron scattering by ^{208}Pb. Although the tails of both curves agree well with each other at the nuclear surface, inside the nucleus the imaginary potentials of the simplified Skyrme version are larger than those of GS2 by up to a factor of 2. The magnitude of the imaginary potential depends on the parameter set of the adopted Skyrme interaction.

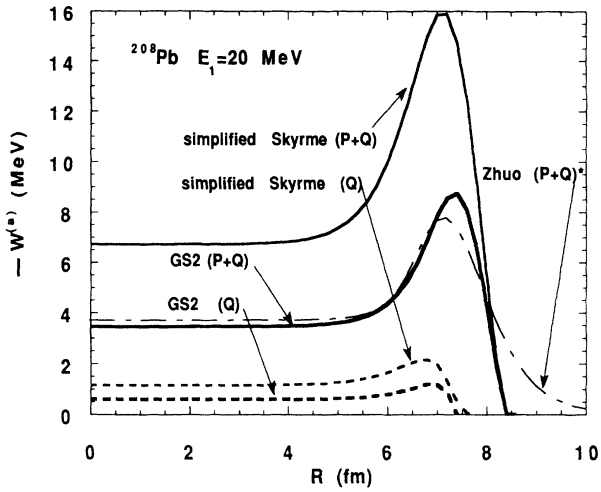

FIG. 15. The imaginary potential based on the GS2 Skyrme force compared with our results based on the simplified delta-type interaction. Zhuo *et al.*'s result denoted by Zhuo $(P + Q)$ is also shown [12].

Comparing our curves with Zhuo *et al.*'s we see that the imaginary potential $W^{(a0)}$ with GS2 agrees with their potential inside the nucleus, but their imaginary potential extends farther out and agrees well with the phenomenological optical potential [20]. This should be due to their adoption of the local density approximation in contrast to our local momentum approximation [8]. In fact, if we define the Fermi wave number $P_F(R)$ by the relation

$$\rho(R) = \frac{2}{3\pi^2} P_F(R)^3, \tag{5.1}$$

we get an imaginary potential $W^{(a0)}$ which extends farther out and is very similar to Zhuo *et al.*'s. The relation (2.4) together with a zero-range interaction make the imaginary potential vanish beyond the classical turning point, although the use of a finite-range interaction makes the imaginary potential extend beyond the classical turning point [8]. As for $W^{(a)}$ both the local density approximation and the local momentum approximation give similar imaginary potentials which fall off rapidly at the nuclear surface due to the restriction to Q space.

To compare with the reaction cross section obtained from phenomenological optical potentials, the reaction cross section for $P + Q$ absorption was calculated for 30 MeV proton scattering by ^{40}Ca and ^{208}Pb and we obtained 900 and 1680 mb, respectively. The values cal-

culated by using the optical potential by Greenlees and Pyle [20] are 940 and 1860 mb, respectively. Our imaginary potential underestimates a little compared with the phenomenological ones, because our potential is cut at the classical turning point although it is larger than the phenomenological one inside the nucleus. So we see that the simplified delta-type interaction gives rather good results, but, to improve our results, more realistic finite-range interactions as well as the inclusion of various higher-order terms are necessary. In a practical application, however, the use of our semiclassical formula for $W^{(a0)}$ and Eq. (5.1) may be useful.

We assumed symmetry with respect to neutrons and protons and chose parameter U_0 as explained before. And we also chose $E_0 = 0$, which may not be a good choice in some cases. For example, protons have a Coulomb barrier so that E_0 may be chosen about the order of magnitude of the barrier height. Except for the process $(a0)$ with $P_0 = \infty$, the magnitude of the imaginary potential is sensitive to the Fermi energy E_F and P_0, because these determine the available phase space for particles. We can estimate the change of g_F with U_0 by dg_F/dU_0 as shown in Table I.

In preequilibrium reactions, the main contribution to absorption comes from process (a), in which particle states should be limited to the Q space. If the conventional imaginary potential in data analyses is used, then the MSC cross section is overestimated. Chadwick and Young [4] analyzed the data of nucleon scattering by ^{93}Nb employing Feshbach *et al.*'s theory [2] and found that the MSC reaction cross section must be reduced by a factor $R^{\rm MSC}$, which is well estimated by the following formula:

$$R^{\rm MSC} = \omega(2p1h, E)/\omega^{P+Q}(2p1h, E) \qquad (5.2)$$

where the numerator ω is the same as that given by (3.3) with $n_p = 2, n_h = 1$, and $\varepsilon_{p\max} = -E_F$, while the denominator ω^{P+Q} is the one with $\varepsilon_{p\max} = \infty$. The ratio is just the portion of intermediate states belonging to Q space. The ratio of the imaginary potential agrees well with the ratio of the state density as shown in Table II.

The effect of absorption of the incoming flux to Q space, however, is measured by the transmission coefficient, which is not proportional to the imaginary potential as shown by (4.1) approximately. In addition, the total contribution comes from many partial waves. In Fig. 13, the ratio of the reaction cross section for Q-space absorption to the one for $P+Q$ absorption was shown together with the imaginary potential ratio $W^{(a)}/W^{(a0)}$ in the case of n+^{93}Nb. Although the reaction cross section is not proportional to the MSC cross section, this indicates that the reduction factor introduced by Chadwick and Young [4] overestimates the effect up to a factor of 2.

TABLE II. Ratio of imaginary potential Q absorption to $P+Q$ absorption, and ratio of state density for Q to $P+Q$ spaces are shown as a function of incident energy for ^{208}Pb.

E (MeV)	$W^{(a)}/W^{(a0)}$	$\omega(2p,1h,E)/\omega^{P+Q}(2p,1h,E)$
0	1	1
10	0.44	0.46
20	0.17	0.20
30	0.083	0.11
40	0.039	0.063
50	0.0083	0.0051

Chadwick and Young [4] emphasized the importance of transitions from the P space to the Q space not only at the first stage but also after collisions in P space. Our second-order results for the transmission coefficient support their claim. However, as already stated, the second-order trasmission coefficient exceeds the unitarity limit. If this is improved by more elaborate calculations, both the direct and second-order transmission coefficients should be reduced to satisfy unitarity.

We see that the most important imaginary potential $W^{(a)}$ is independent of the spectator in the target nucleus. This is the result of neglecting the Pauli blocking effect, or the Pauli principle acting between the produced $2p$-$1h$ state and the existing particles and holes in the target nucleus. To estimate this effect accurately is not easy in our formulation, but a rough estimation is possible. Suppose the total number of states below the Fermi level is N_h and the total state number of particles is N_p. If the target nucleus is a p-particle and h-hole state, the number of combinations making a $2p$-$1h$ state is $\binom{N_p-p}{2}\binom{N_h-h}{1}$ against $\binom{N_p}{2}\binom{N_h}{1}$ for the $0p$-$0h$ state. Then the average reduction factor due to Pauli blocking is given by

$$R_P^{(a)} = \frac{(N_p-p)(N_p-p-1)(N_h-h)}{N_p(N_p-1)N_h}. \qquad (5.3)$$

In Fig. 16 these reduction factors are shown in the cases of ^{40}Ca, ^{93}Nb, and ^{208}Pb as a function of $p = h$. It is seen that this factor becomes important as p increases. Other processes are similarly evaluated, but they are not shown here.

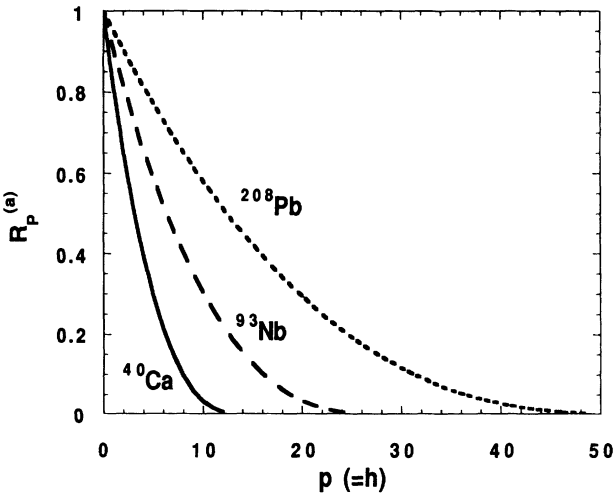

FIG. 16. Imaginary potential reduction factors due to Pauli blocking effect for ^{40}Ca, ^{93}Nb, and ^{208}Pb for process (a) . For ^{40}Ca $N_p = 14, N_h = 20$, for ^{93}Nb $N_p = 26.5, N_h = 46.5$, and for ^{208}Pb $N_p = 51, N_h = 104$ are used.

We have discussed the imaginary part of the optical potential only. The polarization contribution to the real potential may be computed by the dispersion relation if we have the imaginary potential for the whole spectra. However, we have not yet evaluated the one for hole states, so we postpone this discussion until the imaginary potential for hole states is completed.

We have calculated the imaginary potential for fixed particle and hole numbers, but these are connected to the imaginary potential with fixed temperature. This will be discussed in a forthcoming paper.

ACKNOWLEDGMENTS

We thank Professors H. Nishioka and Y. Takahashi, and Dr. M. Abe for stimulating discussions. One of the authors (S.Y.) acknowledges financial support by the Grant-in-Aid for Scientific Research of Japanese Ministry of Education, Science and Culture under Grant No. 04640309.

APPENDIX A: CALCULATION OF INTEGRALS FOR PROCESS (a)

For the calculation of $w^{(a)}$ given by (2.14) it is necessary to evaluate the integral

$$I_a = \int d\mathbf{P}_2 d\mathbf{P}_3 d\mathbf{P}_4 \delta(\mathbf{P}_1 + \mathbf{P}_2 - \mathbf{P}_3 - \mathbf{P}_4) \times \delta(P_1^2 + P_2^2 - P_3^2 - P_4^2) n_h(P_2) n_p(P_3) n_p(P_4). \quad \text{(A1)}$$

After integration over $\mathbf{P}_4$

$$I_a = \int d\mathbf{P}_2 d\mathbf{P}_3 \delta\left[P_1^2 + P_2^2 - P_3^2 - (\mathbf{P}_1 + \mathbf{P}_2 - \mathbf{P}_3)^2\right] \times n_h(P_2) n_p(P_3) \Theta(P_1^2 + P_2^2 - P_3^2 - P_F^2) \times \Theta(P_0^2 - P_1^2 - P_2^2 + P_3^2) \quad \text{(A2)}$$

is obtained. Defining

$$\mathbf{P} = \mathbf{P}_1 + \mathbf{P}_2 = \mathbf{P}_3 + \mathbf{P}_4, \qquad \mathbf{P} \cdot \mathbf{P}_3 = P P_3 \cos\theta_3, \quad \text{(A3)}$$

the first δ function on the right-hand side of (A2) is expressed as

$$\delta\left[P_1^2 + P_2^2 - P_3^2 - (\mathbf{P}_1 + \mathbf{P}_2 - \mathbf{P}_3)^2\right] = \frac{1}{2PP_3}\delta\left(\cos\theta_3 - \frac{P_3^2 + \mathbf{P}_1\mathbf{P}_2}{PP_3}\right). \quad \text{(A4)}$$

As the relation $|(P_3^2 + \mathbf{P}_1 \cdot \mathbf{P}_2)/PP_3| \leq 1$ is shown to be always satisfied, the integral over θ_3 is performed and (A2) becomes

$$I_a = 2\pi \int d\mathbf{P}_2 P_3^2 dP_3 \frac{1}{2PP_3} n_h(P_2) \Theta(P_3 - P_F) \times \Theta(P_0 - P_3) \Theta(P_1^2 + P_2^2 - P_3^2 - P_F^2) \times \Theta(P_0^2 - P_1^2 - P_2^2 + P_3^2). \quad \text{(A5)}$$

The integral over the direction of $\mathbf{P}_2$ is performed by defining

$$\mathbf{P}_2 \cdot \mathbf{P}_1 = P_2 P_1 \cos\theta_2, \quad \text{(A6)}$$

and using the relation

$$\int_{-1}^{1} d\cos\theta_2 \frac{1}{P} = \frac{2}{P_1}. \quad \text{(A7)}$$

The integral range of P_3 is fixed by the step functions in (A5),

$$\max(P_F^2, P_1^2 + P_2^2 - P_0^2) \leq P_3^2 \leq \min(P_0^2, P_1^2 + P_2^2 - P_F^2), \quad \text{(A8)}$$

and the integral over P_3 leads to

$$I_a = \pi^2 \int P_2^2 dP_2 \frac{1}{P_1}\Big[\Theta(P_1^2 + P_2^2 - P_F^2 - P_0^2)\Theta(2P_0^2 - P_1^2 - P_2^2)[P_3^2]_{\sqrt{P_1^2+P_2^2-P_0^2}}^{P_0} + \Theta(P_F^2 + P_0^2 - P_1^2 - P_2^2)\Theta(P_1^2 + P_2^2 - 2P_F^2)[P_3^2]_{P_F}^{\sqrt{P_1^2+P_2^2-P_F^2}}\Big] n_h(P_2). \quad \text{(A9)}$$

The integral range of P_2 is determined by the two step functions and $n_h(P_2)$ in (A9); $P_\alpha \leq P_2 \leq P_\beta$ for the first term and $P_\gamma \leq P_2 \leq P_\delta$ for the second term of the right-hand side of (A9), where $P_\alpha \cdots P_\delta$ are given by (2.17). After performing the integral we finally obtain (2.15).

APPENDIX B: CALCULATION OF INTEGRALS FOR PROCESS (b)

The integral for the process (b) is

$$I_b = \int d\mathbf{P}_3 d\mathbf{P}_4 \delta(\mathbf{P}_1 + \mathbf{P}_2 - \mathbf{P}_3 - \mathbf{P}_4) \times \delta(P_1^2 + P_2^2 - P_3^2 - P_4^2) n_p(P_3) n_p(P_4). \quad \text{(B1)}$$

The calculation is the same as for I_a except for the integral over $\mathbf{P}_2$, and the same definitions (A3) and (A6) are used. We consider two cases according to the magnitude of P_1.

1. $P_0 \leq P_1$

In this case, the relation $|\cos\theta_3| \leq 1$ is always satisfied as in (a) and Eq. (B1) becomes

$$I_b = \frac{2\pi}{2P} \int P_3 dP_3. \quad \text{(B2)}$$

The range of integration over P_3 is given by (A8), but for $P_0 \leq P_1$ it reduces to $P_1^2 + P_2^2 - P_0^2 \leq P_3^2 \leq P_0^2$, and (2.22) is obtained.

2. $P_1 \leq P_0$

In this case, the condition $|\cos\theta_3| \leq 1$ [see Eq. (A4)] gives the relation

$$\left\{P_3^2 - \frac{P_1^2+P_2^2}{2} - \sqrt{\left(\frac{P_1^2+P_2^2}{2}\right)^2 - P_1^2P_2^2\cos^2\theta_2}\right\}\left\{P_3^2 - \frac{P_1^2+P_2^2}{2} + \sqrt{\left(\frac{P_1^2+P_2^2}{2}\right)^2 - P_1^2P_2^2\cos^2\theta_2}\right\} \leq 0. \quad \text{(B3)}$$

Using the notation

$$x = \sqrt{1 - \left(\frac{2P_1P_2}{P_1^2+P_2^2}\right)^2\cos^2\theta_2}, \quad \text{(B4)}$$

(B3) is rewritten as

$$\left\{P_3^2 - \frac{P_1^2+P_2^2}{2}(1+x)\right\}\left\{P_3^2 - \frac{P_1^2+P_2^2}{2}(1-x)\right\} \leq 0, \quad \text{(B5)}$$

where the range of x is given by

$$\alpha \equiv \frac{|P_1^2-P_2^2|}{P_1^2+P_2^2} \leq x \leq 1. \quad \text{(B6)}$$

The range of P_3 is obtained by (A8) together with (B5)

$$\max\left(P_1^2+P_2^2-P_0^2, P_F^2, \frac{P_1^2+P_2^2}{2}(1-x)\right) \leq P_3^2 \leq \min\left(P_1^2+P_2^2-P_F^2, P_0^2, \frac{P_1^2+P_2^2}{2}(1+x)\right). \quad \text{(B7)}$$

Let us consider two cases according to the magnitude of $P_1^2+P_2^2$,

a. $P_F^2 + P_0^2 \leq P_1^2 + P_2^2 \leq 2P_0^2$

Equation (B7) reduces to

$$\max\left(P_1^2+P_2^2-P_0^2, \frac{P_1^2+P_2^2}{2}(1-x)\right) \leq P_3^2 \leq \min\left(P_0^2, \frac{P_1^2+P_2^2}{2}(1+x)\right). \quad \text{(B8)}$$

If $P_1^2+P_2^2-P_0^2 \leq \frac{P_1^2+P_2^2}{2}(1-x)$ holds, then $\frac{P_1^2+P_2^2}{2}(1+x) \leq P_0^2$ also holds. The integral range becomes

$$\frac{P_1^2+P_2^2}{2}(1-x) \leq P_3^2 \leq \frac{P_1^2+P_2^2}{2}(1+x), \quad \text{(B9)}$$

where the range of x is given by

$$\alpha \leq x \leq \beta \equiv \frac{2P_0^2-P_1^2-P_2^2}{P_1^2+P_2^2}. \quad \text{(B10)}$$

The integral (B1) is evaluated as

$$I_b = \frac{\pi}{2P}(P_1^2+P_2^2)x. \quad \text{(B11)}$$

The average over the direction of $\mathbf{P}_2$ is computed by changing the variable $\cos\theta_2$ to

$$P^2 = P_1^2+P_2^2+2P_1P_2\cos\theta_2. \quad \text{(B12)}$$

Noting

$$x = \frac{P\sqrt{2P_1^2+2P_2^2-P^2}}{P_1^2+P_2^2}, \quad \text{(B13)}$$

the average is performed as

$$\bar{I}_b = \frac{1}{2}\int I_b d\cos\theta_2 = \frac{\pi}{4P_1P_2}\left(-\frac{1}{3}\right)\left[(2P_1^2+2P_2^2-P^2)^{3/2}\right]_{P_l}^{P_u}, \quad \text{(B14)}$$

where P_u and P_l are the upper and the lower integral limits of P, respectively. While $\cos\theta_2$ changes from -1 to $+1$, x changes from α to α via $\beta, 1, \beta$. The variable P changes from $|P_1-P_2|$ to P_1+P_2. Corresponding to the first $x=\beta$ and the second β, P takes the values

$$P = P_0 \mp \sqrt{P_1^2+P_2^2-P_0^2}, \quad \text{(B15)}$$

respectively. The integral range of P consists of two parts, namely,

$$|P_1-P_2| \leq P \leq P_0 - \sqrt{P_1^2+P_2^2-P_0^2}$$

and

$$P_0 + \sqrt{P_1^2+P_2^2-P_0^2} \leq P \leq P_1+P_2.$$

Carrying out the integral,

$$\bar{I}_b = \frac{\pi}{4P_1P_2}\frac{1}{3}\left\{6P_>^2P_< + 2P_<^3 - 6P_0^2(P_1^2+P_2^2-P_0^2)^{\frac{1}{2}} - 2(P_1^2+P_2^2-P_0^2)^{\frac{3}{2}}\right\} \quad \text{(B16)}$$

is obtained. Next, the opposite case $\frac{P_1^2+P_2^2}{2}(1-x) \leq P_1^2+P_2^2-P_0^2$ is considered. In this case $P_0^2 \leq \frac{P_1^2+P_2^2}{2}(1+x)$ holds. The integral range is

$$P_1^1+P_2^2-P_0^2 \leq P_3^2 \leq P_0^2 \quad \text{for} \quad \beta \leq x \leq 1, \quad \text{(B17)}$$

and the integral becomes

$$I_b = \frac{\pi}{2P}(2P_0^2-P_1^2-P_2^2). \quad \text{(B18)}$$

The average over the direction $\mathbf{P}$ becomes

$$\bar{I}_b = \frac{\pi}{4P_1P_2}(2P_0^2 - P_1^2 - P_2^2)[P]_{P_l}^{P_u}$$
$$= \frac{\pi}{4P_1P_2}(2P_0^2 - P_1^2 - P_2^2)2\sqrt{P_1^2 + P_2^2 - P_0^2}. \quad \text{(B19)}$$

Adding together (B16) and (B19) the result is given by (2.27).

b. $2P_F^2 \le P_1^2 + P_2^2 \le P_F^2 + P_0^2$

In this case we obtain

$$I_b = \frac{\pi}{2P}(P_1^2 + P_2^2)x \quad \text{for} \quad \alpha \le x \le \gamma, \quad \text{(B20a)}$$

$$I_b = \frac{\pi}{2P}(P_1^2 + P_2^2 - 2P_F^2) \quad \text{for} \quad \gamma \le x \le 1, \quad \text{(B20b)}$$

where

$$\gamma \equiv \frac{P_1^2 + P_2^2 - 2P_F^2}{P_1^2 + P_2^2}. \quad \text{(B21)}$$

Noting

$$P = \sqrt{P_1^2 + P_2^2 - P_F^2} \mp P_F \quad \text{for} \quad x = \gamma, \quad \text{(B22)}$$

the average is carried out just as in the previous case and the result is given by (2.27).

APPENDIX C: CALCULATION OF INTEGRALS FOR PROCESS (c)

For process (c), evaluation of the integral

$$I_c = \int d\mathbf{P}_3 d\mathbf{P}_4 \delta(\mathbf{P_1} - \mathbf{P_2} - \mathbf{P_3} + \mathbf{P_4})$$
$$\times \delta(P_1^2 - P_2^2 - P_3^2 + P_4^2) n_p(P_3) n_h(P_4) \quad \text{(C1)}$$

is necessary. From the energy delta function and two density functions we obtain

$$\max(P_1^2 - P_2^2, P_F^2) \le P_3^2 \le \min(P_1^2 - P_2^2 + P_F^2, P_0^2). \quad \text{(C2)}$$

To carry out integrals over $\mathbf{P}_3$ and $\mathbf{P}_4$ we introduce notations

$$\mathbf{P} = \mathbf{P}_1 - \mathbf{P}_2 = \mathbf{P}_3 - \mathbf{P}_4, \quad \mathbf{P} \cdot \mathbf{P}_3 = PP_3 \cos\theta_3, \quad \text{(C3)}$$
$$\mathbf{P}_1 \cdot \mathbf{P}_2 = P_1P_2 \cos\theta_2.$$

After integration over $\mathbf{P}_4$ the energy delta function yields the relation

$$\delta\left[P_1^2 - P_2^2 - P_3^2 + (\mathbf{P} - \mathbf{P}_3)^2\right]$$
$$= \frac{1}{2PP_3}\delta\left(\cos\theta_3 - \frac{P_1^2 - P_2^2 + P^2}{2PP_3}\right). \quad \text{(C4)}$$

The condition $|\cos\theta_3| \le 1$ leads to $(P_1^2 - P_2^2 + P^2)^2 \le 4P^2P_3^2$, which together with (C2) gives

$$\max\left(P_F^2, \frac{(P_1^2 - P_2^2 + P^2)^2}{4P^2}\right)$$
$$\le P_3^2 \le \min(P_1^2 - P_2^2 + P_F^2, P_0^2) \quad \text{(C5)}$$

as $P_1^2 - P_2^2 \le (P_1^2 - P_2^2 + P^2)^2/4P^2$ is shown to be valid. Equation (2.31) is obtained after integration over $\mathbf{P}_3$. In order to average over the direction of $\mathbf{P}_2$ the integration range of $\cos\theta_2$ must be fixed. The three step functions which appeared in (2.31) give rise to constraints on $\cos\theta_2$. After the integral over $\mathbf{P}_3$ we obtain

$$I_c = 2\pi \int \frac{1}{2PP_3} P_3^2 dP_3 = \frac{\pi}{2P}[P_3^2], \quad \text{(C6)}$$

where the range of P_3 is given by (C5).

Let us consider two cases according to the sizes of $P_0^2 - P_F^2$ and $P_1^2 - P_2^2$.

1. $P_0^2 - P_F^2 \le P_1^2 - P_2^2$

The range of P_3^2 becomes

$$\max\left(P_F^2, \frac{(P_1^2 - P_2^2 + P^2)^2}{4P^2}\right) \le P_3^2 \le P_0^2. \quad \text{(C7)}$$

First consider the following case.

a. $\frac{P_1^2 - P_2^2 + P^2}{2P} \le P_F$

Equation (C6) becomes

$$I_c = \frac{\pi}{2P}(P_0^2 - P_F^2) \quad \text{(C8)}$$

and the range for P is given by

$$P_\beta \le P \le P_\alpha \quad \text{for} \quad P_1^2 - P_2^2 \le P_F^2, \quad \text{(C9)}$$

where

$$P_\alpha = P_F + \sqrt{P_F^2 - P_1^2 + P_2^2}, \quad \text{(C10a)}$$

$$P_\beta = P_F - \sqrt{P_F^2 - P_1^2 + P_2^2}, \quad \text{(C10b)}$$

and the integral averaged over the direction of $\mathbf{P}_2$ becomes

$$\bar{I}_c = \frac{\pi}{2}(P_0^2 - P_F^2)\overline{P^{-1}}$$
$$= \frac{\pi}{2P_1P_2}(P_0^2 - P_F^2)\sqrt{P_F^2 - P_1^2 + P_2^2}. \quad \text{(C11)}$$

Now consider the next case.

b. $P_F \le \frac{P_1^2 - P_2^2 + P^2}{2P}$

Equation (C6) becomes

$$I_c = \frac{\pi}{2P}\left[P_0^2 - \left(\frac{P_1^2 - P_2^2 + P^2}{2P}\right)^2\right], \quad \text{(C12)}$$

and the range for P is given by

$$P_1 - P_2 \le P \le P_1 + P_2 \quad \text{for} \quad P_F^2 \le P_1^2 - P_2^2, \tag{C13a}$$

$$P_1 - P_2 \le P \le P_\beta, \qquad P_\alpha \le P \le P_1 + P_2 \quad \text{for} \quad P_1^2 - P_2^2 \le P_F^2. \tag{C13b}$$

In this case the relation $\frac{P_1^2 - P_2^2 + P^2}{2P} \le P_0$ must be satisfied; this gives the condition

$$P_\delta \le P \le P_\gamma \quad \text{for} \quad P_1^2 - P_2^2 \le P_0^2, \tag{C14}$$

where

$$P_\gamma = P_0 + \sqrt{P_0^2 - P_1^2 + P_2^2}, \tag{C15a}$$

$$P_\delta = P_0 - \sqrt{P_0^2 - P_1^2 + P_2^2}. \tag{C15b}$$

For various values of P the following relations hold:

$$P_1 - P_2 \le P_\delta \le P_\beta \le P_\alpha \le P_\gamma \le P_1 + P_2 \quad \text{for} \quad P_0 \le P_1, \tag{C16a}$$

$$P_\delta \le P_1 - P_2 \le P_\beta \le P_\alpha \le P_1 + P_2 \le P_\gamma \quad \text{for} \quad P_1 \le P_0. \tag{C16b}$$

For $P_0 \le P_1$ combining (C13), (C14), and (C16) we obtain

$$P_\delta \le P \le P_\beta, \quad P_\alpha \le P \le P_\gamma \quad \text{for} \quad P_1^2 - P_2^2 \le P_F^2 \tag{C17}$$

and

$$P_\delta \le P \le P_\gamma \quad \text{for} \quad P_F^2 \le P_1^2 - P_2^2 \le P_0^2. \tag{C18}$$

On the other hand, for $P_1 \le P_0$,

$$P_1 - P_2 \le P \le P_\beta, \quad P_\alpha \le P \le P_1 + P_2 \quad \text{for} \quad P_1^2 - P_2^2 \le P_F^2, \tag{C19}$$

and

$$P_1 - P_2 \le P \le P_1 + P_2 \quad \text{for} \quad P_F^2 \le P_1^2 - P_2^2 \le P_0^2. \tag{C20}$$

Therefore, in the case $P_0 \le P_1$ we have

$$\bar{I}_c = \frac{\pi}{3P_1P_2}(P_0^2 - P_1^2 + P_2^2)^{\frac{3}{2}} \quad \text{for} \quad \max(P_0^2 - P_F^2, P_F^2) \le P_1^2 - P_2^2 \le P_0^2, \tag{C21}$$

and

$$\bar{I}_c = \frac{\pi}{6P_1P_2}\left[2(P_0^2 - P_1^2 + P_2^2)^{\frac{3}{2}} - 2(P_F^2 - P_1^2 + P_2^2)^{\frac{3}{2}} - 3(P_0^2 - P_F^2)\sqrt{P_F^2 - P_1^2 + P_2^2}\right] \quad \text{for} \quad P_0^2 - P_F^2 \le P_1^2 - P_2^2 \le P_F^2, \tag{C22}$$

while for $P_1 \le P_0$

$$\bar{I}_c = \frac{\pi}{6P_1}(3P_0^2 - 3P_1^2 + 2P_2^2) \quad \text{for} \quad \max(P_0^2 - P_F^2, P_F^2) \le P_1^2 - P_2^2 \le P_0^2, \tag{C23}$$

and

$$\bar{I}_c = \frac{\pi}{6P_1P_2}\left[P_2(3P_0^2 - 3P_1^2 + 2P_2^2) - 2(P_F^2 - P_1^2 + P_2^2)^{\frac{3}{2}} - 3(P_0^2 - P_F^2)\sqrt{P_F^2 - P_1^2 + P_2^2}\right] \quad \text{for} \quad P_0^2 - P_F^2 \le P_1^2 - P_2^2 \le P_F^2. \tag{C24}$$

2. $P_1^2 - P_2^2 \le P_0^2 - P_F^2$

This case applies only for $P_1 \le P_0$ and Eq. (C4) becomes

$$\max\left(P_F^2, \frac{(P_1^2 - P_2^2 + P^2)^2}{4P^2}\right) \le P_3^2 \le P_1^2 - P_2^2 + P_F^2. \tag{C25}$$

First consider the following case.

a. $\frac{P_1^2 - P_2^2 + P^2}{2P} \le P_F$

Equation (C6) becomes

$$I_c = \frac{\pi}{2P}(P_1^2 - P_2^2), \tag{C26}$$

and the range for P is given by

$$P_\beta \le P \le P_\alpha \quad \text{for} \quad P_1^2 - P_2^2 \le P_F^2, \tag{C27}$$

and the integral averaged over the direction of $\mathbf{P}_2$ becomes

$$\bar{I}_c = \frac{\pi}{2P_1P_2}(P_1^2 - P_2^2)\sqrt{P_F^2 - P_1^2 + P_2^2}. \tag{C28}$$

Now consider the next case.

b. $P_F \le \frac{P_1^2 - P_2^2 + P^2}{2P}$.

Equation (C6) becomes

$$I_c = \frac{\pi}{2P}\left(P_1^2 - P_2^2 + P_F^2 - \frac{(P_1^2 - P_2^2 + P^2)^2}{4P^2}\right). \tag{C29}$$

In this case $P_1^2 - P_2^2 + P_F^2 - \frac{(P_1^2 - P_2^2 + P^2)^2}{4P^2} \ge 0$ holds. For $P_F^2 \le P_1^2 - P_2^2$ the integration range is given by

$$P_1 - P_2 \le P \le P_1 + P_2, \tag{C30}$$

and averaged integral is

$$\bar{I}_c = \frac{\pi}{6P_1}(3P_F^2 - P_2^2)$$

$$\text{for} \qquad P_F^2 \le P_1^2 - P_2^2 \le P_0^2 - P_F^2. \quad \text{(C31)}$$

In the opposite case $P_1^2 - P_2^2 \le \min(P_0^2 - P_F^2, P_F^2)$, the integration range is

$$P_1 - P_2 \le P \le P_\beta, \quad P_\alpha \le P \le P_1 + P_2, \quad \text{(C32)}$$

and the averaged integral is given by

$$\bar{I}_c = \frac{\pi}{6P_1P_2}\Big[P_2(3P_F^2 - P_2^2) - (P_1^2 - P_2^2 + 2P_F^2)\sqrt{P_F^2 - P_1^2 + P_2^2}\Big]$$

$$\text{for} \quad P_1^2 - P_2^2 \le \min(P_F^2, P_0^2 - P_F^2). \quad \text{(C33)}$$

Adding the obtained results, the final forms are summarized as follows: for $P_0 \le P_1$,

$$\bar{I}_c = \frac{\pi}{3P_1P_2}[(P_0^2 - P_1^2 + P_2^2)^{\frac{3}{2}}\Theta(P_0^2 - P_1^2 + P_2^2) - (P_F^2 - P_1^2 + P_2^2)^{\frac{3}{2}}\Theta(P_F^2 - P_1^2 + P_2^2)], \quad \text{(C34)}$$

and for $P_1 \le P_0$,

$$\bar{I}_c = \frac{\pi}{6P_1P_2}\Big[P_2(3P_0^2 - 3P_1^2 + 2P_2^2)\Theta(P_1^2 - P_2^2 - P_0^2 + P_F^2) + P_2(3P_F^2 - P_2^2) \times\Theta(P_0^2 - P_F^2 - P_1^2 + P_2^2) - 2(P_F^2 + P_2^2 - P_1^2)^{3/2}\Theta(P_F^2 - P_1^2 + P_2^2)\Big]. \quad \text{(C35)}$$

In deriving the above formula the following averages over angle θ_2 are used

$$\overline{P} = \left(\frac{P^3}{6P_1P_2}\right)_{P_l}^{P_u}, \quad \overline{P^{-1}} = \left(\frac{P}{2P_1P_2}\right)_{P_l}^{P_u}, \quad \overline{P^{-3}} = \left(\frac{-P^{-1}}{2P_1P_2}\right)_{P_l}^{P_u}, \quad \text{(C36)}$$

where P_l and P_u indicate the lower and upper limits of P.

APPENDIX D: CALCULATION OF INTEGRALS FOR PROCESS (d)

We evaluate the integral

$$I_d = \int d\mathbf{P}_4\delta(\mathbf{P}_1 - \mathbf{P}_2 - \mathbf{P}_3 + \mathbf{P}_4) \times\delta(P_1^2 - P_2^2 - P_3^2 + P_4^2)n_h(P_4). \quad \text{(D1)}$$

Using Eq. (C3) we obtain

$$I_d = \frac{1}{2P_3P}\delta\left(\cos\theta_3 - \frac{P_1^2 - P_2^2 + P^2}{2PP_3}\right). \quad \text{(D2)}$$

From the condition $|\cos\theta_3| \le 1$ we obtain the range

$$-1 < \alpha < \cos\theta_2 < \beta < 1, \quad \text{(D3)}$$

where

$$\alpha = \frac{P_1^2 - P_3^2 - P_3\sqrt{P_2^2 + P_3^2 - P_1^2}}{P_1P_2}, \quad \text{(D4a)}$$

$$\beta = \frac{P_1^2 - P_3^2 + P_3\sqrt{P_2^2 + P_3^2 - P_1^2}}{P_1P_2}. \quad \text{(D4b)}$$

The average over the direction of $\mathbf{P}_3$ yields

$$\bar{I}_d = \frac{1}{4}\int \frac{1}{2P_3P}d\cos\theta_2. \quad \text{(D5)}$$

By using (D3) the average over the direction of $\mathbf{P}_2$ is performed and (2.36) is obtained.

APPENDIX E: CALCULATION OF INTEGRALS FOR PROCESS (e)

The integral

$$I_e = \int d\mathbf{P}_4\delta(\mathbf{P}_1 + \mathbf{P}_2 - \mathbf{P}_3 - \mathbf{P}_4) \times\delta(P_1^2 + P_2^2 - P_3^2 - P_4^2)n_p(P_4) \quad \text{(E1)}$$

is evaluated. Using (A3) and (A6) the integral over $\mathbf{P}_4$ is carried out,

$$I_e = \frac{1}{2PP_3}\delta\left(\cos\theta_3 - \frac{P_3^2 + P_1P_2\cos\theta_2}{PP_3}\right). \quad \text{(E2)}$$

From the condition $|\cos\theta_3| \le 1$ the region of $\cos\theta_2$ is fixed as

$$1 < -\alpha \le \cos\theta_2 \le \alpha < 1, \quad \text{(E3)}$$

where

$$\alpha = \frac{P_3\sqrt{P_1^2 + P_2^2 - P_3^2}}{P_1P_2}. \quad \text{(E4)}$$

Averaging over the direction of $\mathbf{P}_3$

$$I_e = \frac{1}{4PP_3}, \quad \text{(E5)}$$

and further averaging over the direction of $\mathbf{P}_2$

$$\bar{I}_e = \frac{1}{4P_1P_3}, \quad \text{(E6)}$$

from which Eq. (2.42) is obtained.

[1] S. Yoshida, Proc. Phys. Soc. (London) Ser. A **69**, 668 (1956).
[2] H. Feshbach, A. K. Kerman, and S. Koonin, Ann. Phys. **125**, 429 (1980).
[3] R. Bonetti, M. B. Chadwick, P. E. Hodgson, B. V. Carlson, and M. S. Hussein, Phys. Rep. **202**, 171 (1991).
[4] M. B. Chadwick and P. G. Young, Phys. Rev. C **47**, 2255 (1993).
[5] H. Nishioka, J. J. M. Verbaarschot, H. A. Weidenmüller, and S. Yoshida, Ann. Phys. (N.Y.) **172**, 67 (1986).
[6] J. J. M. Verbaarschot, H. A. Weidenmüller, and M. R. Zirnbauer, Phys. Lett. C **129**, 367 (1985).
[7] M. Herman, G. Reffo, and H. A. Weidenmüller, Nucl. Phys. **A536**, 124 (1992).
[8] R. W. Hasse and P. Schuck, Nucl. Phys. **A438**, 157 (1985).
[9] P. Grange, J. Cugnon, and A. Lejeune, Nucl. Phys. **A473**, 365 (1987).
[10] S. Hayakawa, M. Kawai, and K. Kikuchi, Prog. Theor. Phys. **13**, 41 (1955); E. Clement and C. Villi, Nuovo Cimento **2**, 176 (1955).
[11] P. Ring and P. Schuck, *The Nuclear Many-Body Problem* (Springer, New York, 1980).
[12] Zhuo Yizhong, Shen Qingbiao, and Tian Ye, Adv. Sci. China Phys. **1**, 231 (1985).
[13] S. Yoshida and H. Morinaga, Z. Phys. A **317**, 173 (1984).
[14] G. Peilert, H. Stöcker, and W. Greiner, Phys. Rev. C **39**, 1402 (1989).
[15] A. Bohr and B. R. Mottelson, *Nuclear Structure* (Benjamin, New York,1969), Vol. 1.
[16] C. Mahaux, P. F. Bortignon, R. A. Broglia, and C. H. Dasso, Phys. Rep. **120**, 1 (1985).
[17] P. Obložinský, Nucl. Phys. **A453**, 127 (1986); K. Stankiewicz, A. Marcinkowski, and M. Herman, *ibid.* **A435**, 67 (1985); C. Kalbach, Report No. LA-10248-MS, Feb, 1985.
[18] Y. Takahashi and S. Yoshida, Nucl. Phys. **A507**, 371 (1990).
[19] H. Nishioka, H. A. Weidenmüller, and S. Yoshida, Z. Phys. A **336**, 197 (1990).
[20] G. W. Greenlees and G. J. Pyle, Phys. Rev. **149**, 836 (1966).